Chemical Aspects of Three-Dimensional Photonic Crystals

Jun Hyuk Moon*,† and Shu Yang*,‡

Department of Chemical and Biomolecular Engineering, Sogang University, 1 Shinsu-dong, Mapo-gu, Seoul 121-742, Korea, and Department of Materials Science and Engineering, University of Pennsylvania, 3231 Walnut Street, Philadelphia, Pennsylvania 19104

Received March 1, 2009

Contents

1. Introduction 547
2. Chemistry for 3D Fabrication of Photonic Structures 549
   2.1. Block Copolymer Assembly 549
   2.2. Colloidal Assembly 550
      2.2.1. Synthesis of Colloidal Particles 550
      2.2.2. Coating and Assembly of Colloidal Crystals 551
      2.2.3. Assembly of Binary Colloidal Particles 553
   2.3. Interference Lithography 553
      2.3.1. Multibeam Interference Lithography (MBIL) or Holographic Lithography (HL) 554
      2.3.2. Phase Mask Interference Lithography (PMIL) 554
      2.3.3. Photoresists for Optical Interference Lithography 555
   2.4. Two-Photon Lithography (TPL) 560
      2.4.1. Two-Photon Photoinitiators 561
      2.4.2. Photosensitive Materials Used in Two-Photon Lithography 562
      2.4.3. Introducing Controlled Defects in Photonic Crystals 564
3. Backfilling Chemistry 565
   3.1. Chemical Vapor Deposition (CVD) 566
   3.2. Atomic Layer Deposition (ALD) 567
   3.3. Sol−Gel Reactions 567
   3.4. Supercritical Deposition 569
   3.5. Electrochemical Deposition 569
   3.6. Chemical Reduction 569
4. Summary and Outlook 570
5. Acknowledgments 570
6. References 571

1. Introduction

Three-dimensional (3D) photonic crystals (PCs) are crystalline materials where the refractive index is periodically modulated on a length scale comparable to the light wavelength of interest. Interference of the light waves scattered from the dielectric lattice (i.e., Bragg scattering) leads to omnidirectional stop bands or photonic band gaps (PBGs), which are analogous to the electronic energy band gaps in a semiconductor.[1,2] The bandwidth and the frequency of the PBG are determined by the refractive index contrast between the high and low (typically air) dielectric materials, the structural symmetry and periodicity, and the filling fraction and morphology of high-refractive-index materials. Photonic crystals with a large, complete PBG are highly desired, which act like an optical trap to reflect incident light from any direction at a certain frequency range of light. Thus, controlled functional structures can be engineered into the 3D structures to confine or guide photons of specific wavelengths. Therefore, PCs potentially offer revolutionary advances in the next-generation microphotonic devices and the integration of existing optoelectronic devices, including integrated optical circuits, lasers, sensing, spectroscopy, and pulse shaping. In the last two decades, there has been much interest in exploring new PC structures and studying the related new phenomenon. Existing techniques for the large-scale fabrication of microstructures with submicrometer features mainly rely on the use of optical projection lithography developed for silicon IC manufacturing. This method is inherent 2D patterning and requires laborious layer-by-layer photolithography and etching processes or stacking and fold-up of the 2D layers to generate the continuous 3D structures.[2−4] A promising 3D fabrication technique should be able to do the following:

- produce submicrometer periodicity for PBGs in the visible to infrared (IR) spectral range
- access a large number of structures with tailored shapes, functionalities, and sizes of motifs
- allow for mass-production over a large area
- provide fine control of defects for photonic device applications
- construct structures from materials with high refractive indices for complete PBGs.

In recent years there has been a considerable effort to develop novel methods for mass production of 3D PCs with controlled size, symmetry, and defect(s) on a large scale basis (see Table 1). They can be categorized into self-assembly and lithography-based techniques. Self-assembly approaches, such as crystallization of colloidal particles[5] or emulsions, and microphase separation of block copolymers[6] or surfactants, are simple, mass-producible, and least expensive. However, it is inevitable to introduce random defects, such as missing particles, uncontrolled orientation, mixture of phases, and dislocations during the self-assembly processes. In addition, the type of lattice from colloidal assembly is rather limited, typically exhibiting face-centered-cubic (fcc) symmetry. In comparison, the lithography-based techniques, including three-axis micropositioner assisted deposition of polymer melts and solutions (e.g., rapid prototyping,[7] pressure assisted microsyringe deposition,[8] focused-ion-beam etching,[9] direct-write assembly[10]), layer-by-layer stacking through conventional photolithography[2] or soft lithography,[11−13] and glancing angle deposition (GLAD),[14,15] often require

* To whom correspondence should be addressed. E-mail addresses: J.H.M., junhyuk@sogang.ac.kr; S.Y., shuyang@seas.upenn.edu.
† Sogang University.
‡ University of Pennsylvania.

10.1021/cr900080v
Published on Web 08/05/2009

Jun Hyuk Moon obtained his B.S. degree in 1999 in Chemical Engineering from Korea University (Seoul, Korea). He obtained his M.S. in 2001 and his Ph.D. degree in 2005 in Chemical and Biomolecular Engineering from Korea Advanced Institute of Science and Technology (KAIST) under the supervision of Prof. Seung-Man Yang. During his Ph.D. studies, he worked as an exchange graduate student with Prof. David J. Pine at the University of California, Santa Barbara. Following postdoctoral research with Prof. Shu Yang at the Department of Materials Science and Engineering, University of Pennsylvania, he joined Samsung Advanced Institute of Technology as a member of the R&D staff in 2007. In 2008, he joined the Department of Chemical and Biomolecular Engineering at Sogang University as an assistant professor. His current research includes design, synthesis, and application of hierarchical porous materials for optical sensors, photoelectrochemical electrodes, and superhydrophobic surfaces.

Shu Yang received her B.S. degree in Materials Chemistry from Fudan University, China, in 1992, and her Ph. D. degree from Chemistry and Chemical Biology under the supervision of Professor Christopher K. Ober in the Department of Materials Science and Engineering at Cornell University in 1999. She then joined Bell Laboratories, Lucent Technologies as a Member of Technical Staff before moving to the Department of Materials Science and Engineering at University of Pennsylvania in 2004, where she now is an Associate Professor. She also holds a secondary appointment in the Department of Chemical and Biomolecular Engineering at University of Pennsylvania. Her current research includes synthesis and engineering of well-defined polymers and inorganic materials with controlled size, shape, and morphology over multiple length scales, study of their unique surface, optical, and mechanical properties, surface functionalization and dynamic tuning on topographic surfaces, biomimetic mineralization on functional polymer templates, directed-assembly in solution and on patterned surfaces, and creating complex patterns via harnessing elastic instability. She has received an ICI award (1999) and Unilever award (2001) for outstanding research in polymer science and engineering from the ACS, selection to "Frontier of Engineering" by the National Academy of Engineering (2002), and MIT's Technology Review TR35 (2004). She received the Faculty Early Career Development (CAREER) award from National Science Foundation (NSF) in 2006.

multiple steps to create any single structure. The advantage, though, is that they are highly suitable to create structures with arbitrary complexity. It will be ideal if we can combine the benefits of mass-production using self-assembly approaches and the long-range ordering using lithographic processes. A few nonconventional lithography approaches based on a parallel optical interference process, including multibeam or multifaced prism interference lithography,[16−23] and phase mask interference lithography,[24−32] have shown promise for the rapid production of highly periodic 3D structures with submicrometer periodicity that are defect-free over a large area (up to cm^2). Through single or multiple exposures (for a few nanoseconds to seconds), the size and shape of the fabricated structures can be conveniently controlled through the proper arrangement of laser beams or the grating in the phase mask. On the other hand, two-photon lithography is well suited for constructing arbitrarily shaped 3D microstructures and precise defect structures through direct laser writing using a femtosecond laser.[33−37]

Although there has been a race in fabrication of a wide range of 3D PCs for applications in visible to IR regions, no complete PBG has been observed experimentally in the directly fabricated 3D crystals from polymers or silica. This is because in addition to periodicity and volume filling fraction, the appearance of a complete PBG and its width is highly dependent on the refractive index contrast. Among every Bravais lattice and symmetry that have been explored, theoretical calculation suggests that the diamond lattice is the champion PC possessing the largest complete PBGs.[38−40] Yet a minimum refractive index contrast of 1.9 is necessary to open a complete PBG in diamond.[39,41] In contrast, most patterned films from polymer or silica have low refractive index contrast ($n < 1.7$). Therefore, materials properties have become the more pressing issues that limit the practical realization of 3D PCs in optical devices. To address this concern, a number of templating approaches have been investigated, which use the fabricated polymer or silica structures as templates for backfilling of high-refractive-index inorganic materials, followed by removal of the template, resulting in inverse 3D inorganic or semiconducting PCs (see detailed discussion in section 3). Meanwhile, PCs with tunable band gaps offer promise in applications that do not require complete PBGs, such as reflective displays,[42,43] chemical/biological and optical sensors,[44−49] optical shutters, and active filters and polarizers.[50−56] For this purpose, polymeric or silica structures can be utilized through surface functionalization or a templating method. For example, we can engineer or tune the band gap by infiltrating functional materials, such as metallic or magnetic nanoparticles,[57−61] liquid crystals,[43,62,63] and stimuli responsive gels.[44,45,49,64−69] Regardless of the fabrication/backfilling approaches, it is critical to control materials chemistry to create desired 3D structures with preferred materials properties, for example, high refractive index, high transmission at the wavelength of interest, wide tunability, and high thermal and mechanical stability. There have been several comprehensive reviews on various 3D fabrication techniques to create photonic band gap structures, including microphase separation of block copolymers,[70] colloidal assembly,[5,71] interference lithography,[22,23] and two-photon lithography.[35−37] However, few have reviewed the backfilling chemistry and fidelity in template fabrication and backfilling processes (e.g., lattice distortion, pattern collapse, incompleteness of backfilling, and crack formation). In this review, we focus on the chemical aspects in fabrication of high-refractive-index 3D PCs, especially the recent advancement and breakthrough in large area fabrication with high fidelity. First, we present the chemistry

Table 1. Comparison of Different Types of 3D Microfabrication Techniques

technique	materials	pros	cons	ref
self-assembly (SA)	•monodispersed polymeric or inorganic particles	•a wide range of pattern sizes (10 nm − a few μm)	•slow (seconds to days)	5, 71
	•block copolymers	•inexpensive	•limited to fcc lattice in the case of colloid assembly	6, 39, 80−82
		•large pattern dimension (10 cm × 10 cm)	•random defects	
interference lithography (IL)	•photosensitive polymers (organic and hybrids)	•various lattice symmetries,	•periodic structures only	16, 17, 20, 22, 23
		•fast (nanoseconds to a few seconds)		
		•pattern dimension (10 cm × 10 cm)		
		•nearly defect-free		
two-photon lithography (TPL)	•photosensitive monomeric liquids, polymer films (organic, hybrids)	•arbitrary patterns	•slow (several mm/s), serial writing	33, 35−37, 203
		•nearly defect-free	•low spatial resolution (>100 nm)	
			•limited pattern dimension (100 μm × 100 μm)	
direct-write assembly (DWA)	•polyelectrolyte	•arbitrary patterns	•slow (250 μm/s)	10, 276
	•concentrated colloidal gels, and •nanoparticle gels	•nearly defect-free	•low spatial resolution (>100 nm) •pattern dimension (1 cm × 1 cm)	
glancing angle deposition (GLD)	•semiconductors	•direct patterning of semiconductors, metals, or metal oxides	•high vacuum process	14, 15
	•metals •metal oxides	•nearly defect-free	•slow (2−10 Å/s) •limited lattice structures	

and recent advances in 3D fabrication of high quality photonic structures and in design of stimulus-responsive materials for dynamic tuning of photonic properties. We then discuss various backfilling chemistries, including chemical vapor deposition (CVD), atomic layer deposition (ALD), sol−gel reactions, supercritical deposition, electrochemical deposition, and chemical reduction.

2. Chemistry for 3D Fabrication of Photonic Structures

Various fabrication methods, including self-assembly, the standard microelectronic fabrication process, and nonconventional optical lithography, have been pursued to create various 3D microstructures with submicrometer periodicity in a controlled manner. While the layer-by-layer techniques, such as stacking via conventional photolithography[2] or soft lithography,[11−13] and GLAD,[14,15] are capable of direct production of 3D PCs with high refractive index contrast, these methods are laborious and expensive and often lack control of random defects. Here, we focus on review of several fabrication techniques that can create 3D photonic structures rapidly and inexpensively over a large area, including the self-assembly of block copolymers and colloidal particles, optical interference lithography, and direct-writing techniques, and the chemical issues in fabrication.

2.1. Block Copolymer Assembly

Block copolymers (BCPs) consist of two or more chemically different polymers (or blocks), which are covalently linked together at the junction of two blocks. The positive enthalpy of mixing and low mixing entropy of the constituent blocks drive the local segregation, often referred to as microphase separation, of the blocks into domains since macroscopic phase separation is restricted. At equilibrium, the BCP chains will be arranged in minimum free energy configurations, which are determined by the chemical incompatibility (or segment−segment interaction parameter, χ) and composition, whereas the domain size is dependent on the molecular weight of different polymer segments, typically on the order of 10−100 nm. In the case of AB diblock copolymers, we could expect at least four thermodynamically equilibrium morphologies, including spherical, cylindrical, gyroid, and lamellar structures.[72] By adding a third block, a wealth of one-, two-, and three-dimensional periodic dielectric structures (at least twelve) can be obtained with more complex morphologies.[73] Therefore, microphase separation of block copolymers has been of great interest as a simple yet efficient method to pattern a wide range of wafer-size nanostructures in comparison to the expensive photolithography processes for smaller and faster semiconductor devices.[74−79]

Theoretical analysis of the BCP morphologies suggests that there exists directional PBGs in these structures.[39,70,80−82] Specifically, 3D periodic bicontinuous cubic structures, including single primitive, single diamond, and single gyroid level surfaces, have shown large complete PBGs, and the lowest index contrast (∼1.9) to open a band gap is slightly lower than that of dielectric or air spheres on a diamond lattice.[39] Because of the accessible length scale (10−100 nm), BCPs are mostly interested for applications in visible and UV spectra.[6,81,82] For example, Urbas et al. have fabricated porous nanostructures with gyroid networks from polystyrene-*b*-polyisoprene (PS-*b*-PI) copolymers by selective etching of polyisoprene block. Their calculation shows that gyroid PC is comparable to diamond PC, which can open a complete PBG with the refractive index contrast of about 2.3.[40,83]

One major drawback of BCPs for practical applications, however, is that these self-assembled structures are often trapped in the nonequilibrium states on the pathway to minimize the energy barrier, thus making it difficult to achieve desired structures with long-range ordering, which is critical for many practical applications. Various attempts have been demonstrated to improve the ordering and orientation of the block copolymer nanostructures on a substrate, as well as to control the feature size, including tuning solvent

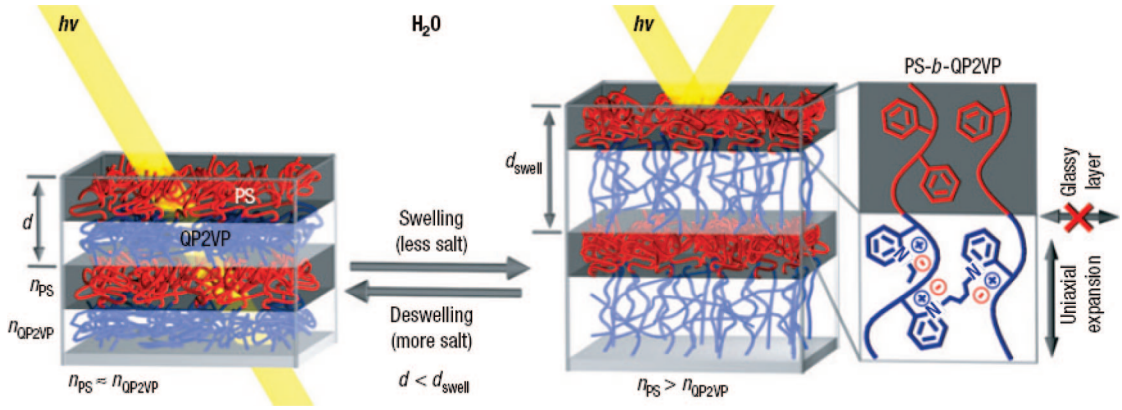

Figure 1. Schematic diagram of the structure of a photonic gel film and the tuning mechanism. The photonic gel film was prepared by self-assembly of a diblock copolymer (PS-b-QP2 VP). Swelling/deswelling of the QP2 VP gel layers (blue) by aqueous solvents modulates both the domain spacing and the refractive-index contrast, and accordingly shifts the wavelengths of light ($h\nu$) reflected by the stop band. The hydrophobic and glassy polystyrene layers (red) limit expansion of the gel layers to the direction normal to the layers. (Reprinted from ref 100. Copyright 2007 Nature Publishing Group.)

evaporation rate,[84] directed assembly on lithographically defined templates,[75,77,85,86] application of an external field (e.g., electric, magnetic, and shearing force),[87−94] and annealing the film above its glass transition temperature or through solvent-induced swelling.[95,96]

While it remains challenging to control random defects, grain boundaries, and orientation for device applications, one outstanding advantage of the BCP assembly is its flexibility to tune photonic properties, for example, by loading various nanoparticles or introducing stimulus-responsive materials.[97−99] Thermoresponsive band gap switching has been demonstrated from the mixture of poly(styrene-*b*-4-vinylpyridium methanesulphonate) (PS-*b*-P4 VP) and 3-*n*-pentadecyl phenol (PDP).[99] Since the hydrogen bonding between PDP and PS-*b*-P4 VP can be reversibly tuned, an on−off switching of stop band can be achieved by varying environmental temperature. Recently, Kang et al. have shown broad-wavelength range tunabilility by using a hydrophobic block-hydrophilic polyelectrolyte block polymer, polystyrene-*b*-quaternized poly(2-vinylpyridine) (PS-*b*-QP2 VP) (Figure 1).[100] Compared to previous works using colloidal assemblies, which typically show a shift of stop band ∼100−200 nm,[101,102] the lamella gel formed by the PS-*b*-QP2 VP shows >1250 nm reversible shifts by swelling/deswelling of the QP2 VP gel layer in aqueous solvent (Figure 2a). Further, the swelling can be reduced by osmotic deswelling in a salt solution; thus, the stop band can be tuned from UV to near-infrared (NIR) simply by varying the salt concentration (Figure 2b).

2.2. Colloidal Assembly

Similar to BCP assemblies, colloidal assembly is a low-cost and low-energy consumption method to fabricate 3D photonic structures. The method is based on the self-assembly of monodispersed colloidal particles into ordered crystalline structure (see Figure 3). The assembly process is scalable to an area over square centimeters, and the periodicity of PCs can be tuned simply by varying the particle size from hundreds of nanometers to micrometers. Equilibrium configurations of colloidal assemblies are randomly close-packed in general, while early experiments and simulations have shown that fcc packings are favored over hexagonally close-packed (hcp) structures even though the free energy difference between them is miniscule, on the order of $0.001kT$/particle.[103−109]

The application of colloidal crystals, however, could be hampered by the difficulty of controlling long-range ordering, similar to the BCP assembly, and the difficulty of creating structures beyond fcc lattices. The competition between fcc and hcp structures during colloidal particle packing has led to the appearance of random defects, including vacancies, macroscopic cracks, polycrystalline domains, and stacking faults. Several mechanisms have been proposed to explain the role of different forces in the assembly of ordered 3D colloidal crystals, which is nicely reviewed by Norris et al.[110] More recent work has explored approaches to improve the quality of colloidal crystals. To this end, we particle size distribution and will overview the impact of surface characteristics, solvent, and deposition methods on the assembly of high quality colloidal crystals.[111]

2.2.1. Synthesis of Colloidal Particles

Most high quality colloidal crystals are assembled from monodispersed polystyrene (PS), poly(methylmethacrylate) (PMMA), and silica particles with submicrometer size.[112] This is because large particle size variation can easily disrupt the crystalline lattice. Simulation shows that high quality colloidal crystals can be formed if the particle size is within 2% of standard deviation.[113] As the size distribution increases, the intensity reflectance by the stop band decreases rapidly. The complete PBG in the inverted structures disappears completely when the standard deviation of particle diameter is greater than ∼5%.

The polymeric particles are typically prepared by emulsion polymerization and dispersion polymerization.[114] Additional functionalities can be introduced during the synthesis of colloidal particles.[115] For example, photoprocessable colloids of poly(*tert*-butylmethyacrylate)[116] and poly(styrene-*co*-glycidyl methacrylate)[117] have been prepared to introduce defect structures directly in the opal crystals through a UV lithography process and to photo-cross-link the polymer opals to create hierarchical arrays of nanopores, respectively.

Monodispersed silica particles are synthesized by sol−gel reaction of tetraorthosilicate (TEOS) precursors using the Stöber method.[118] Hybrid silica particles with narrow size distribution (< ±2%) have been prepared by addition of triethoxysilanes (RTES) or trimethoxysilanes (RTMS), where the organic substitute R represents methyl, phenyl, octyl, and vinyl groups. Nevertheless, colloidal crystals assembled from

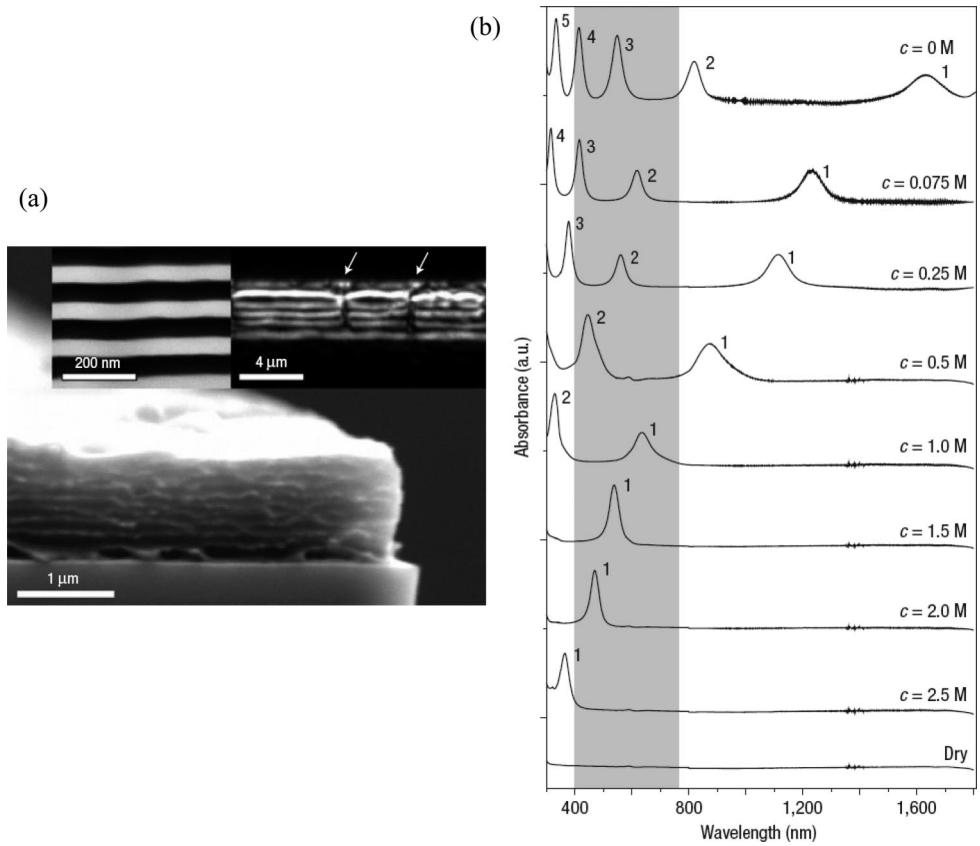

Figure 2. Photonic gel film. (a) SEM micrograph of a dry PS-b-QP2 VP lamellar photonic film deposited on a silicon wafer. The left TEM inset image is the same film stained with I_2 vapor (dark layers are I_2-stained QP2 VP domains). The right inset image is a reflection-mode laser-scanning confocal microscope image (*xz* scan) of a swollen film showing defect channels (marked by arrows) across the layers. (b) Ultraviolet−visible−near-infrared absorbance spectra of PS-b-QP2 VP photonic gels swollen by contact with different concentrations of NH_4Cl aqueous solution. The gray region represents the visible wavelength region. (Reprinted from ref 100. Copyright 2007 Nature Publishing Group.)

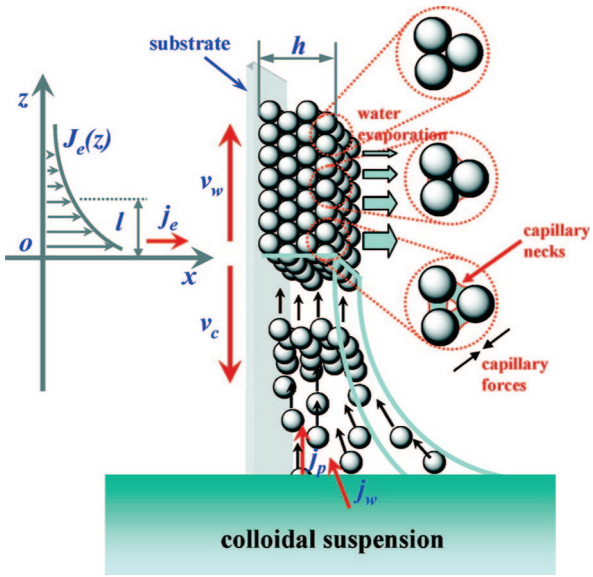

Figure 3. Schematic presentation of the particle and water fluxes in the vicinity of multilayer particle arrays growing on a substrate plate that is being withdrawn from a colloidal solution. (Reprinted from ref 125. Copyright 2007 American Chemical Society.)

polymer or (hybrid) silica particles are often used as templates for backfilling of high-refractive-index semiconductor materials and responsive gels. A detailed discussion of backfilling chemistry and the fidelity will be presented later in section 3.

Colloidal particles prepared from high-refractive-index semiconductors, such as CdS, ZnS ($n > 2.5$, transparent in the NIR region), and TiO_2 ($n > 2.0$, transparent in the visible wavelengths), are preferred for complete PBGs. However, it is challenging to synthesize monodispersed semiconductor colloids due to the relatively high reactivity of the precursors. It has been suspected that the hydrolysis rate of these precursors is too fast such that it is difficult to separate the nucleation and growth steps.[119] Therefore, nucleation events occur continuously through the entire sol−gel process, leading to the formation of polydispersed particles. In the case of titania, the monodispersed particles have been synthesized by controlling hydrolysis of glycolated titanium butoxide in acetone and using surfactant as a stabilizer (Tween 20).[120] Particle size to within tens of nanometers has been demonstrated by varying the concentrations of titanium butoxide and surfactant.

2.2.2. Coating and Assembly of Colloidal Crystals

Equilibrium configurations of colloidal assemblies are randomly close-packed, although slow sedimentation favors fcc packings over hcp structures. Nonequilibrium hydrodynamic interactions on settling and colloidal particle interactions might drive the formation of fcc packings. Most practical applications of colloidal crystals require the colloidal particles to be assembled on substrates in a relatively short period of time. Various processes, including sedimentation, vertical dip-coating deposition, infiltration in the capillary, epitaxial growth on a patterned substrate, and spin-coating,

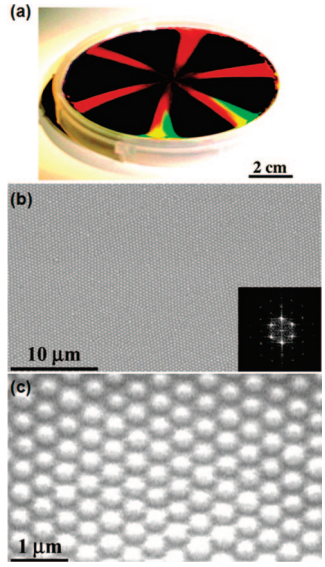

Figure 4. (a) Photograph of a 3D ordered nanocomposite film on a 4-in. silicon wafer illuminated with white light. The sample is made from 325 nm diameter colloidal spheres. (b,c) Typical scanning electron microscope (SEM) images of a spin-coated colloidal crystal−polymer nanocomposite film. The inset shows a Fourier transform of a 40 × 40 μm^2 region. (Reprinted from ref 129. Copyright 2004 American Chemical Society.)

have been developed.[121−124] Most of them are based on evaporation-driven convective assembly. In the case of the vertical deposition, the substrate is withdrawn from the colloidal solution or the solvent is evaporated by controlling the temperature gradient to move down the meniscus level. The deposition begins with the pinning of the colloidal particle on the menisci region, and then other colloidal particles move to the pinned particle by the water influx from water evaporation. Finally, they assemble into ordered structures driven by capillary force, which is mediated by a bridging meniscus as shown in Figure 3.[125] The number of colloidal layers can be estimated as[125]

$$k = \frac{\beta l}{0.605 d v_w + \Gamma'} \frac{j_e \varphi}{(1 - \varphi)} \quad (1)$$

where β is the ratio between the velocity of a particle in solution and fluid velocity, l is the meniscus height, d is the diameter of the particles, v_w is the substrate withdrawal rate, Γ' is the water volume flux between particles, j_e is the water evaporation flux, and φ is the particle volume fraction. According to eq 1, the thickness of colloidal crystals can be controlled in an experiment by varying the volume fraction of the colloidal solution and the withdrawing rate. Recently, the colloidal crystal growth has been interpreted in terms of the convective steering hypothesis,[110,111,126] which suggests that solvent flow into and through the pore space of the crystal may play a major role in the assembly. However, this method is limited to film thickness no more than 20 μm.

Further, external forces, such as the shear effect, the electric field, and infrared heating, can be applied to increase the quality of colloidal crystals.[127] Kanai et al. showed the pressure-driven shear alignment in crystalline colloids, resulting in high spectral quality and centimeter-sized colloidal crystals.[128] Jiang et al. have demonstrated formation of wafer-size colloidal crystals from silica spheres with uniform thickness and long-range ordering simply by spin-coating the colloidal silica particle solution (see Figure 4) dispersed in a mixture of a viscous, nonvolatile monomer, ethoxylated trimethylolpropane triacrylate (ETPTA) (∼20 vol %), and a photoinitiator.[129−131] Because of the refractive index and density matching between silica and ETPTA, the van der Waals attraction and sedimentation are greatly reduced, resulting in stable colloids. During the spin-coating, the particles were assembled into non-close-packed crystals filled with ETPTA, and the crystallization is achieved by shear-induced ordering. The monomers surrounding the particles are photopolymerized to provide mechanical support to the film. The high shear rates (>10^5/s) exert high centrifugal and viscous forces to the particles; therefore, hexagonally packed colloidal layers are readily formed. However, the requirement of a viscous monomer solution as a dispersion medium adds length in fabrication steps, which could limit the application of the spin-coating technique to other colloidal particle systems. Later, Mihi et al. have reported a modified spin-coating technique by dispersing the silica and sulfonated polystyrene microspheres in different mixtures of volatile solvents, including ethanol, water, and ethylene glycol.[132] The key is to control the volatility of the solvent such that it will allow enough time for particles to order by shearing but practically evaporate within a few minutes. Compared to the method of Jiang et al., this approach offers better stability against aggregation and no additional selective etching is needed to obtain a colloidal crystal with high dielectric contrast. The viscosity and volatility of the solution can be controlled by varying the ratio of solvents and the concentration of particles in order to control the thickness and orientation of colloidal crystal films with respect to the substrate. To address the crack formation due to volume shrinkage during the drying of the colloidal crystal films, Wang et al. have employed a mixture solution of silica particles and silica precursor (from an acidic tetraethyl orthosilicate (TEOS) solution) for dip-coating.[133] The interstices between silica beads are filled with hydrolysis produced silica species to prevent crack formation, which can be selectively removed by exposure to hydrofluoric acid vapor.

For the stability of colloids in solution and their assembly, it is critical to control the interparticle potentials, which are influenced by the surface charge of colloidal particles and the surrounding media, such as pH, salt concentration, and ionic strength. For example, in the case of silica particles synthesized by sol−gel reactions, the presence of silanol groups on a particle surface causes electrostatic repulsion between particles. Due to the weakly acidic silanol groups, silica particles are positively charged in water at a pH below 1.5 and become negatively charged at a pH above 3.5.[134] The negative surface charge can be further enhanced by addition of a base.[135−137] Yamanaka et al. showed the charge-induced crystallization to obtain one-directional crystal growth over centimeter size regions. They applied a weak base, pyridine, through a gel membrane, and the colloidal particles are assembled by the increase of surface charge along the diffusion of the base (see Figure 5).[135] Meanwhile, adding salt could diminish the range of repulsive electrostatic forces.[138] In the study of crystallization confined in 2D, Rodner et al. show that the domain size of colloidal crystals decreases exponentially with the increase of salt concentration.[139] Bevan et al. study the effect of ionic strength systematically by using confocal scanning laser microscopy in real-time.[138] They conclude that the high ionic strength can rupture the crystalline phase, leading to disordered structures. By varying the surface chemistry, one can

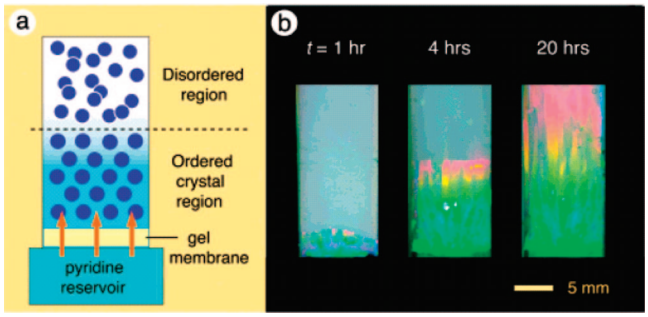

Figure 5. (a) Experimental system and (b) images of the one-directional growth process. (Reprinted from ref 135. Copyright 2004 American Chemical Society)

Table 2. Maximum Photonic Band Gap Width of Colloidal PCs of Silicon (Refractive Index Contrast of Silicon−Air, 3.41) (Adapted from Ref 145)

structure	gap/midgap %	volume filling fraction, *f*
tetrastack	13.7	0.43
inverted tetrastack	25.3	0.21
diamond	12.9	0.41
inverted diamond	26.9	0.2
inverted fcc	4.8	0.28

optimize the colloidal assembly and create responsive PCs. The latter has been utilized as pH and ionic strength sensors for detection of chemical and biological species.[44−46,49,64,140−142]

2.2.3. Assembly of Binary Colloidal Particles

Theoretically, inverted fcc arrays of air spheres in a high refractive index medium (refractive index contrast, >2.9) have been shown to possess a complete PBG in the visible wavelength. However, only a limited number of materials possess both high refractive index and transparency in visible light, including titania (rutile phase)[143] and Sb_2S_3.[144] Further, the growth of crystalline titania in the rutile phase requires a high sintering temperature, ~900 °C, leading to the formation of cracks due to thermal shrinkage and growth of the crystalline domain. Recent work reveals that, among various sphere-based PCs, the diamond and tetrastack structures are most favorable for large complete PBGs, as summarized in Table 2.[145] By numerical phase-diagram analysis, Hynninen et al. proposed to fabricate both diamond and tetrastack structures via assembly of binary colloidal particles.[146] The binary spheres can be mixed to form Laves phases, which is analogous to the atomic lattice of $MgCu_2$, $MgZn_2$, or $MgNi_2$ crystals (Figure 6a−c). Specifically, in the phase diagram, there is a stable state of Laves structures, as shown in Figure 7. In the case of $MgCu_2$ (Figure 6d), the lattice consists of a diamond structure of large spheres and a tetrastack structure of small spheres. Therefore, the selective removal of spheres can form both lattices (Figure 6e,f). However, the authors also showed that the three different Laves structures possess a similar free-energy difference to that of the colloidal crystal with the same-sized spheres, which often forms a random hexagonal close-packed crystal. A few Laves structures have been observed experimentally from the assemblies of nanometer-sized particles.[147] While it remains challenging to assemble highly ordered colloidal crystals from several hundred nanometer diameter particles, Leunisssen et al. have reported a breakthrough by charge-induced assembly of binary colloidal crystals.[148] They applied apolar colloids to match the density and refractive index and to avoid sedimentation and van der Waals attraction. The

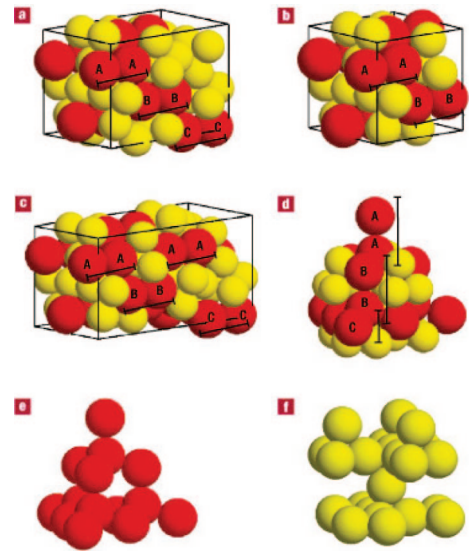

Figure 6. Large spheres are red, and small spheres are yellow. (a) MgCu2. (b) MgZn2. (c) MgNi2. (d−f) The $MgCu_2$ structure. Part d is a combination of a diamond structure of large spheres (e) and a tetrastack structure of small spheres (f). (Reprinted from ref 146. Copyright 2007 Nature Publishing Group.)

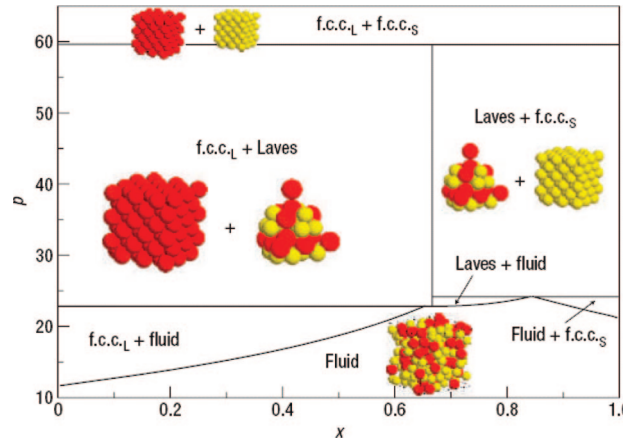

Figure 7. The phase diagram is shown in the composition *x*, reduced pressure *p*, representation, where $x = N_S/(N_S + N_L)$ is the number fraction of small spheres. The labels "'fcc_L" and "fcc_S" denote the fcc crystals of large and small particles, respectively. There are stable Larves structures where the pressure region $p = 22.8-59.6$ and the composition $x = 0.667$. (Reprinted from ref 146. Copyright 2007 Nature Publishing Group.)

charges of the particles were fine-tuned by adding surfactants of opposite and dissimilar charges to avoid irreversible aggregation. The assembled lattices showed almost the same sizes from a mixture of large and small particles. Even with micrometer-sized spheres, the authors were able to show various equilibrium phases, analogous to the atomic lattices of CsCl and NaCl. Nevertheless, challenges remain in large-scale production and assembly of such binary particles on a substrate for photonic device applications.

2.3. Interference Lithography

In comparison to self-assembly approaches, top-down lithographic processes are intrinsically free of random defects. Periodic structures can be fabricated in photoresists by optical interference lithography, including (1) focusing multiple coherent beams (multibeam interference, MBIL, or holographic lithography, HL)[16,17,19−23,181] and (2) interference of

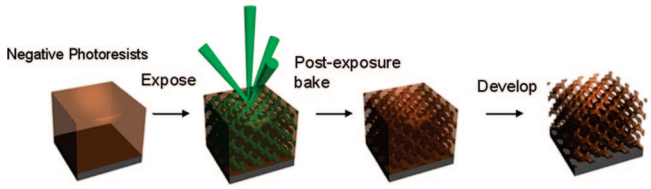

Figure 8. Schematic illustration of a holographic lithography process using an umbrella-like four beam setup, forming diamond-like interference patterns. When the interference pattern is subjected to a negative-tone photoresist, the exposed regions are cross-linked, whereas unexposed or weakly exposed regions are removed by a developer, resulting in a microporous 3D photonic structure.

diffracted beams passing through a grating, so-called phase mask interference lithography (PMIL).[24−32,149]

2.3.1. Multibeam Interference Lithography (MBIL) or Holographic Lithography (HL)

When n (≥ 2) coherent optical waves are present simultaneously in the same region of space, the waves interfere and generate periodic variations in intensity if the difference between the wave vectors is noncoplanar.[150] The intensity distribution of the interference field can be described by a Fourier superposition

$$I(\mathbf{r}) = \sum_{l=1}^{n}\sum_{m=1}^{n} \boldsymbol{\varepsilon}_l \boldsymbol{\varepsilon}_m^* \exp i(\mathbf{k}_l - \mathbf{k}_m)\mathbf{r} \propto \sum_{l=1}^{n}\sum_{m=1}^{n} a_{lm} \exp i(\mathbf{G}_{lm}\mathbf{r}) \quad (2)$$

where $\mathbf{r}$ is the position vector and $\mathbf{k}$ and $\boldsymbol{\varepsilon}$ are the wave vector and polarization vector, respectively. $a_{lm} = \boldsymbol{\varepsilon}_l \boldsymbol{\varepsilon}_m^*$ is the magnitude and $G_{lm} = \mathbf{k}_l - \mathbf{k}_m$ is the difference between two of the laser-beam wave vectors. G_{lm} determines translational symmetry, and G_{lm} together with $\boldsymbol{\varepsilon}_n$ determine symmetries present in the structure (i.e., space group). Interference among any n (≤ 4) noncoplanar laser beams produces an intensity grating with $(n - 1)$ dimensional periodicity. The symmetry of the resulting structures can be controlled by the wave vectors and polarizations of the interfering beams. When subjecting this light intensity profile to a photoresist, the exposed region will be polymerized/cross-linked (negative-tone) or decomposed (positive-tone) based on the same photochemistry used in the conventional lithography,[151] resulting in formation of a periodic 3D structure without the use of a photomask (see Figure 8). HL can rapidly produce a large volume of artificial micrometer polymer crystals rather efficiently at ambient temperature in a single exposure step (nanoseconds to seconds) that are defect-free in an area up to several square centimeters. Moreover, HL is mask-free and versatile: one can change the beam geometry to create various periodic 3D optical structures that are normally difficult to access by other microfabrication techniques, although for some structures the optical setup could be complex. To simplify the optical setup, multifaceted prisms are often implemented.[21,68,152] The porosity (10−80%) and pore size (~100 nm to a few micrometers) can be varied conveniently by changing the beam intensity, the exposure time, or the concentration of base additives. A wide range of functional 2D and 3D periodic structures with a variety of lattice symmetries, including hexagonal biomimetic microlens arrays with integrated pores,[153] fcc,[17,18] simple cubic (P), diamond (D), diamond-like, and gyroid (G) structures,[19−21,154] quasi-crystals[149,155,156] and compound structures,[157,158] with periods of 0.3−6 μm, have been demonstrated both theoretically and experimentally.

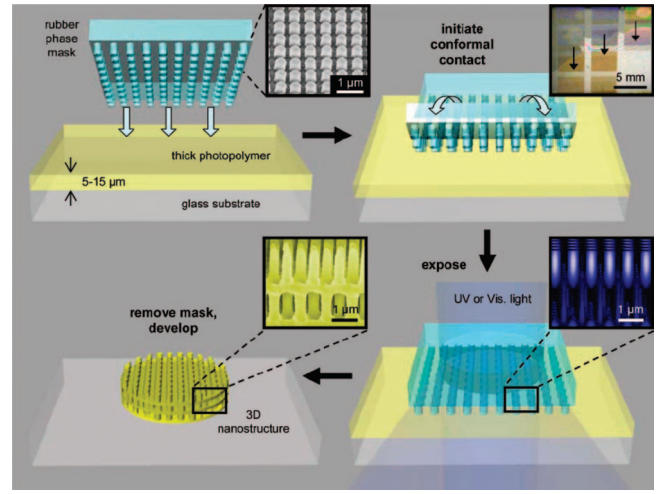

Figure 9. Schematic illustration of steps for using a high-resolution conformable, elastomeric phase mask to produce 3D structures. Placing such a mask (upper left) on the surface of a solid photopolymer film leads to intimate, conformal contact (upper right). Shining light through the mask (lower right) generates a complex intensity distribution throughout the thickness of the film (inset). Interaction of the light with the polymer results in cross-linking reactions. Washing away the uncross-linked polymer yields 3D patterns (lower left). (Reprinted from ref 24. Copyright 2004 The National Academy of Sciences of the USA).

2.3.2. Phase Mask Interference Lithography (PMIL)

Mass production of 3D crystals by MBIL, however, could be limited by (1) the accessible size of the unit cell, which is fixed once the beam geometry (incidence angles and polarization vectors) is chosen for a certain crystal symmetry, and (2) the expandable laser beam size (typically a few millimeters in diameter). Using triple exposure of a pair of beams, a simple cubic structure with variable size has been demonstrated by changing the angles between the beams of the individual gratings.[20] However, multiple exposures could be constrained by the accessible optical setups and nonlinear optical response in photoresists. PMIL has been recently developed to create 3D structures with a wide range of symmetry and size over a large area.[24−32,159] Figure 9 illustrates the PMIL placing a conformal, elastomeric phase mask from poly(dimethylsiloxane) (PDMS) on a solid photoresist film to produce 3D structures. It is based on diffraction of light through an optical phase mask and therefore is a single-exposure, single-beam lithographic technique. When illuminating the phase mask with a normally incident, monochromatic beam, it produces a multibeam diffraction pattern throughout the film thickness, where the exposed regions will be cross-linked and the uncross-linked regions will be washed away by an organic solvent, yielding a 3D pattern. The phase mask can be replica molded from a patterned Si master, an approach commonly used in soft lithography. The conformal contact of the PDMS mask with the photoresist film allows mass-production of a 3D film over 10 cm in diameter and up to 100 μm thick.[24]

The number of beams per diffracted order is usually determined by the rotational symmetry of the 2D phase mask. For example, a 2D square lattice phase mask produces four beams per order. It is noted, however, that the more propagating beams in the exposure region, the smaller the

Table 3. Typical Photoresist Systems Used in Interference Lithography

Photoresists		Chemistry Structure	Pros	Cons	Ref
Negative-tone	SU-8	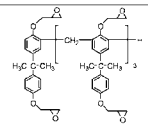	• ultrathick films • high resolution and contrast • commercially available	• large volume shrinkage	176
	PGMA	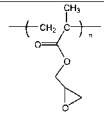	• low volume shrinkage	• low refractive index	178
	Sol-gel composites	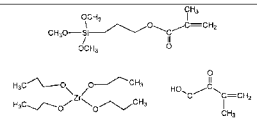	• high refractive index	• limited loading of inorganic component • low pattern contrast	182
	POSS	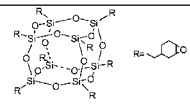	• convertible to silica	• liquid film, • low pattern contrast	186,208,277
	PHEMA copolymers	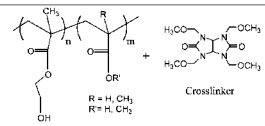	• biocompatible • responsive	• low pattern contrast	68,69,190
Positive-tone	AZ5214	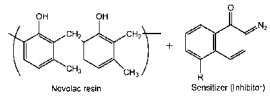	• low volume shrinkage • removable by organic solvent • high contrast	• limited to thin film • sensitive to environment	22,69

contrast of the 3D intensity pattern, and the more challenge to obtain the structure in the recording photoresist. To improve lithographic contrast, it is necessary to design the phase mask, allowing for only the lowest diffracted order modes to propagate in the exposed region, while keeping all higher order modes evanescent.

2.3.3. Photoresists for Optical Interference Lithography

A variety of photosensitive materials, including negative-tone and positive-tone organic−inorganic hybrids and responsive hydrogels, have been investigated to fabricate 3D photonic structures using optical interference lithography. The chemical structures and their applications have been summarized in Table 3.

Negative-Tone Photoresist, SU-8. In optical interference lithography, the negative-tone photoresist SU-8, a bisphenol-A novolac resin derivative with an average of eight epoxy groups per monomer,[160] is most commonly used. It is highly soluble in many organic solvents, which enables preparation of ultrathick films (up to 2 mm),[161,162] and is highly transparent in the near-UV and visible region.[161] Upon exposure to UV or visible light, SU-8 becomes highly cross-linked and exhibits excellent thermal (T_g > 200 °C) and mechanical (Young's modulus E up to 5.0 GPa) strength. Therefore, it has been widely used to fabricate microelectromechanical systems (MEMS) devices,[163] microfluidic channels,[164] high-aspect ratio (≥20) microstructures,[161,162,165−167] 3D photonic structures,[16−18,22] and substrates for biological applications.[168,169] Commercially available SU-8 photoresists (Microchem Inc.) consisting of EPON SU-8 (from Shell Chemicals) and triaryl sulphonium salts as UV photoacid generators (PAGs) are dissolved in γ-butyrolactone (GBL) or cyclopentanone (CP).

In a typical interference lithography process, the SU-8 solution is spun onto a transparent substrate (e.g., cover glass) and prebaked on a hot plate at 95 °C to evaporate the solvent. During exposure, the PAGs release photoacids, followed by a postexposure bake at 95 °C to accelerate acid diffusion, resulting in cationic polymerization of the epoxy groups in SU-8. The unexposed film is then removed by the developer propylene glycol methyl ether acetate (PGMEA). The relatively high glass transition temperature of SU-8 photoresists, 50 °C, plays an important role in minimizing the acid diffusion before the postexposure bake. A high glass transition temperature has been one of the key resist design criteria to achieve submicrometer resolution in deep UV lithography of chemically amplified photoresists. It is equally important in interference lithography, since polymerization during exposure is not desired: it would disturb the original interference pattern due to the change of refractive index of the cross-linked film. When the film is exposed at room temperature and then baked at 95 °C, the beam interference stage is separated from the film cross-linking stage.

Although SU-8 resin is quite transparent in the near-UV region, it is more appealing to perform interference lithography using visible light. Not only is the visible continuous wave (cw) laser more readily accessible in the lab than the UV pulse laser, but the longer wavelength is also advantageous to realize a larger lattice period. Further, the transmission of the photoresists increases significantly in the visible region; therefore, interference of visible light (i) is more flexible and applicable to a wide range of photosensitive materials and (ii) provides a more even exposure throughout

Scheme 1. General Scheme for Photosensitized Cationic Polymerization (Reprinted from ref 17. Copyright 2002 American Chemical Society.)

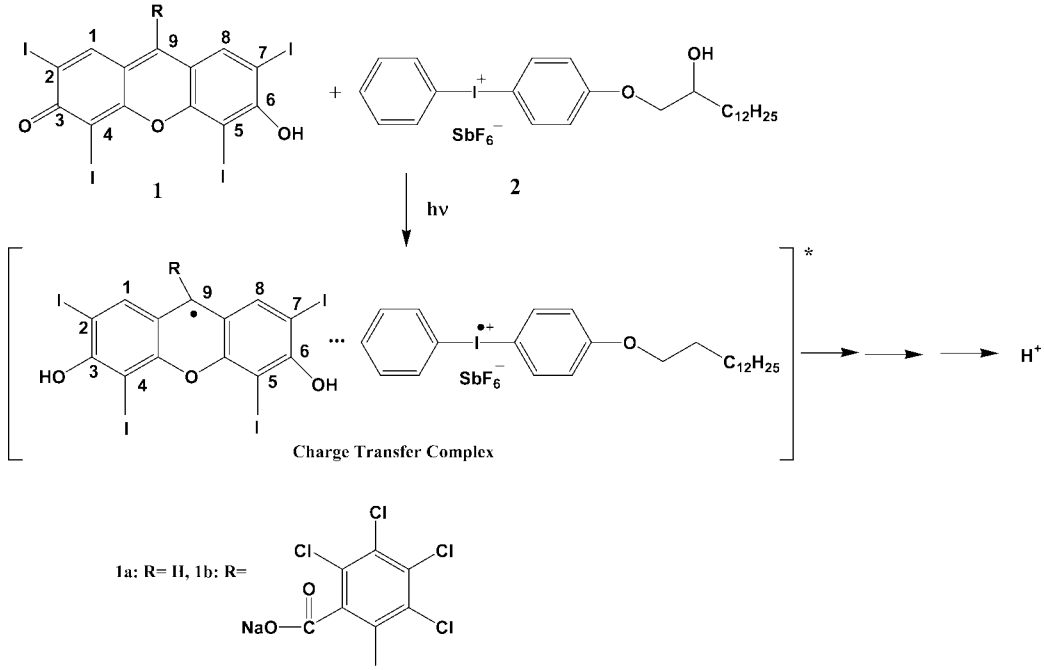

Scheme 2. Different Photoinitiating Systems for Photoacid Generation at the Visible Wavelength

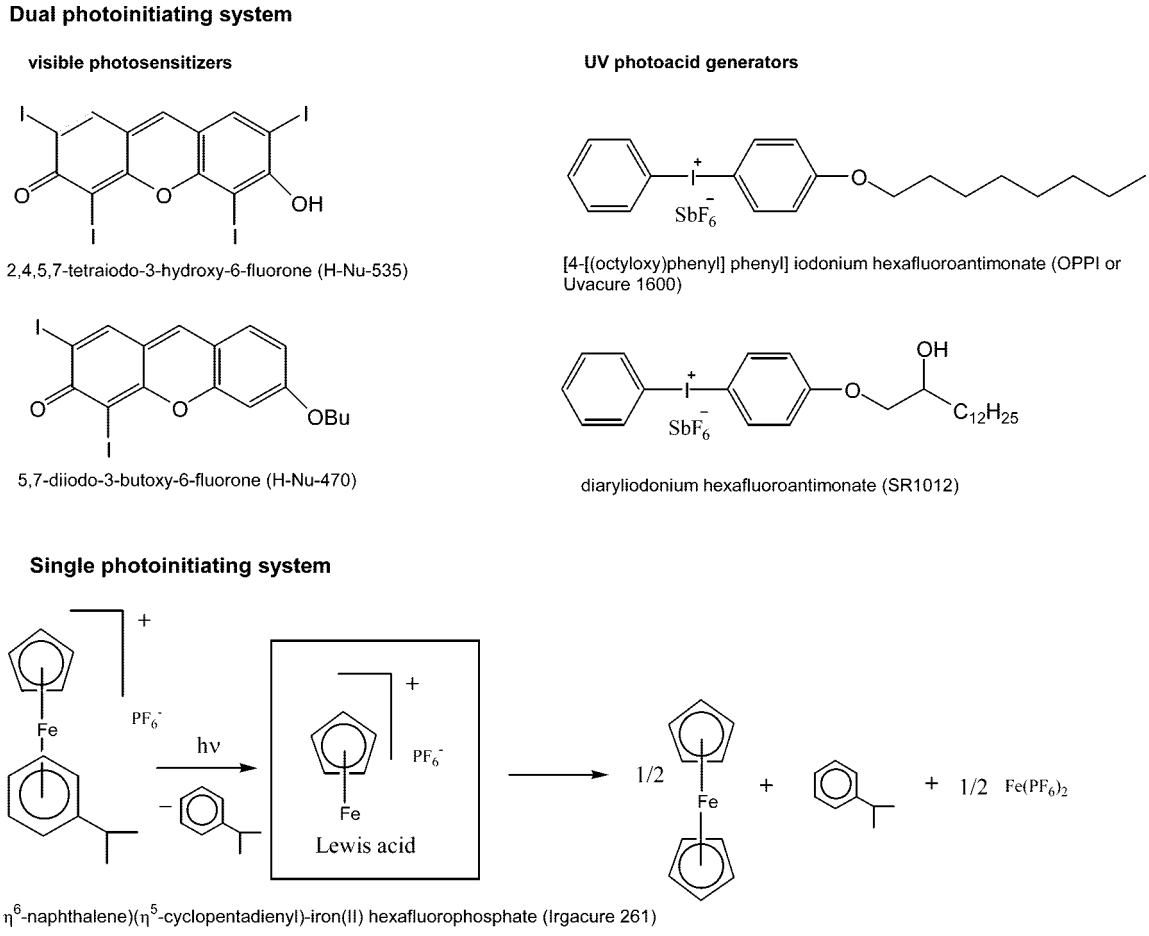

the thick films and better control of the interference pattern. Since most of the photoacid generators do not have absorption at visible wavelengths, the initiating system typically includes a photosensitizer, which absorbs the visible light and electron transfers to an onium salt via the formation of a charge transfer complex to generate the acids (see Scheme 1).[170−172] Typically diaryliodonium salts instead of triarylsulfonium salts are chosen as photoacid generators due to the low reduction potential of iodionium salts for energy transfer. The photoacids initiate ring-opening reactions of

Table 4. Lattice Parameters for the Interference Patterns in Air and SU-8 ($c = 2\pi$/d and $d = 1.38\ \mu$m) (Reprinted from ref 176. Copyright 2007 Optical Society of America.)

Medium	Air	SU8 (considering refraction effect only)	SU8 (considering both refraction and film shrinkage)
Reciprocal lattice vectors	$\vec{b}_1 = c[-1, 1, 1]$; $\vec{b}_2 = c[1, -1, 1]$; $\vec{b}_3 = c[1, 1, -1]$.	$\vec{b}'_1 = c[-1.140, 0.860, 0.860]$; $\vec{b}'_2 = c[0.860, -1.140, 0.860]$; $\vec{b}'_3 = c[0.860, 0.860, -1.140]$;	$\vec{b}''_1 = c[-1.006, 0.994, 0.994]$; $\vec{b}''_2 = c[0.994, -1.006, 0.994]$; $\vec{b}''_3 = c[0.994, 0.994, -1.006]$;
Real lattice vectors	$\vec{a}_1 = 0.5d[0, 1, 1]$; $\vec{a}_2 = 0.5d[1, 0, 1]$; $\vec{a}_3 = 0.5d[1, 1, 0]$.	$\vec{a}'_1 = 0.743d\ [0.327, 1, 1]$; $\vec{a}'_2 = 0.743d\ [1, 0.327, 1]$; $\vec{a}'_3 = 0.743d\ [1, 1, 0.327]$;	$\vec{a}''_1 = 0.506d\ [0.013, 1, 1]$; $\vec{a}''_2 = 0.506d\ [1, 0.013, 1]$; $\vec{a}''_3 = 0.506d\ [1, 1, 0.013]$;
Plot of real lattices	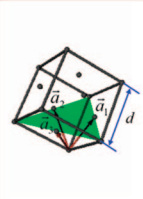	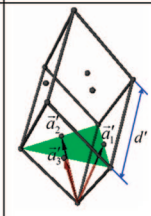	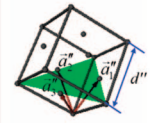
Translational symmetry	fcc	rhombohedral	rhombohedral
Lattice constant d (μm)	1.38	1.78	1.39
$\lvert\vec{a}_j\rvert$ (μm)	0.98	1.49	0.99
Angle between $\vec{a}_i$ & $\vec{a}_j$	60°	38.3°	59.1°
Distance between the nearest lattice points in (111) plane (μm)	0.98	0.98	0.98
Distance between the adjacent lattice planes in [111] direction h_{111} (μm)	0.80	1.38	0.81
Space groups of the corresponding level surfaces	No. 166 ($R\bar{3}m$)	No.155 ($R32$)	No.155 ($R32$)

epoxy groups, and the acids are regenerated in the subsequent steps.[170] The polymerization is thus chemically amplified, resulting in a highly cross-linked film. Several visible photosensitizer/PAG systems for the SU-8 photoresist have been studied (see Scheme 2), including xanthene dyes, 2,4,5,7-tetraiodo-6-hydroxy-3-fluorone (H-Nu 535 from Spectra Group Ltd.), and diaryliodionium hexafluoroantimonate (SR1012 from Sartomer),[17] 5,7-diiodo-3-butoxy-6-fluorone (H-Nu 470 from Spectra Group Ltd.), and [4-[(octyloxy)phenyl]phenyl]iodonium hexafluoroantimonate (OPPI from Spectra Group Ltd. or Uvacure 1600 from UCB Chemicals Corp.).[29,173,174] A single photoinitiation system, (η^6-naphthalene)(η^5-cyclopentadienyl)iron(II) hexafluorophosphate (Irgacure 261 from Ciba Specialty Chemicals), which has weak absorption in visible light and generates Lewis acids upon exposure, is also demonstrated.[153,154,175]

Low-Shrinkage, Negative-Tone Photoresists. During HL experiments, the influence of refraction at the air/film interface cannot be ignored when the beams travel from the air into the resist film. This problem may be addressed by the use of prisms and/or index matching liquids to precompensate the effects of refraction.[21] However, it is not uncommon to observe large shrinkage of the photoresists during photoexposure and development, especially in the case of negative-tone resists. Thus, the fabricated structure may possess a different lattice symmetry and periodicity from the original design, which in turn may affect the quality of PBGs.[176] For example, a large volumetric shrinkage (as high as ca. 41%; see Table 4) has been observed in the diamond-like SU-8 structure after postexposure baking (PEB) and development, leading to the decrease of the translational symmetry from fcc in air to rhombohedral in SU-8, and the overall symmetry of the lattice changed from space group No. 166 ($R\bar{3}m$) in air to No. 155 ($R32$) in SU-8.[176] Furthermore, if the film is attached to the substrate, cracks may occur and propagate due to the residual strain generated from large film shrinkage, further degrading the optical quality of PCs.

While the percentage of shrinkage can be tuned by varying the exposure dosage and PEB time and temperature fundamentally, the shrinkage is caused by the increase of film density during the polymerization, where the van der Waals

Table 5. Comparison between Volumetric Shrinkage of PGMA (DP = 35) and SU-8 under the Same Fabrication Conditions (Reprinted from ref 178. Copyright 2008 Royal Society of Chemistry)

	PGMA (n = 1.52, DP = 35)		SU-8 (n = 1.60)	
materials	pitch in the (111) plane	distance between the adjacent lattice planes in the [111] direction	pitch in the (111) plane	distance between the adjacent lattice planes in the [111] direction
experimental (μm)	1.05	1.07	0.97	0.81
calculated* (μm)	0.98	1.30	0.98	1.38
shrinkage (%)	−7.1	18	1.0	41
volume shrinkage (%)	5.9	42		

* Obtained from a level surface by considering the influence of refraction at the photoresist film/air interface.

separation of monomer units is replaced by covalent bonds. In addition, during development, the organic solvent would swell the cross-linked film, which further distorts the patterned film after drying. We note that the distortion caused by resist shrinkage is different from the pattern collapse caused by capillary force exerted during development, rinsing, and drying steps, which is dependent on the wetting contact angle, the surface tension of the developer/rinsing solvent, and the pattern geometry. For the later, it can be addressed by the use of supercritical drying[17,24] or the selection of a solvent with a sufficiently large contact angle.[177] However, these methods do not alleviate the film shrinkage, which is dependent on the level of functionality involved in photo-cross-linking and the related film cross-linking density.

One approach to address the film shrinkage is to design highly branched multifunctional monomers such that formation of only a few bonds can lead to a dramatic switching of solubility, thus simultaneously improving viscosity and lowering film shrinkage. Dendrimeric methacrylates are examples of branched monomers. Still, there is generally a volume shrinkage of ~15 − 20% using vinyl monomers. Recently, Hayek et al.[178] used an epoxy-based system with a controllable number of epoxy groups in an effort to optimize the trade-offs between solubility of the resin for good film formation and number of epoxy groups required to switch solubility. Using the atom-transfer radical polymerization method, they synthesized poly(glycidyl methacrylate) (PGMA) with well-controlled average molecular weights and narrow molecular weight distributions. The shrinkage of PGMA materials was measured from SEM images. As seen from Table 5, the 3D structure fabricated from PGMA (degree of polymerization, DP = 35) shows much lower shrinkage (18%) in the [111] direction in comparison to that from SU-8, 41%. In the (111) plane, while the SU-8 structure had ~1% shrinkage, PGMA structures (DP = 35) showed 7.1% expansion. Overall, the volume shrinkage of the 3D structure is 5.9% for PGMA films, much lower than that from SU-8, 42%. For both PGMA and SU-8 templates, the anisotropic shrinkage in different directions can be attributed to the substrate confinement effect, where the porous structure can shrink freely in the vertical direction but is restricted in the horizontal plane. Compared with the SU-8 material, the PGMA material always shows a higher pitch in the (111) plane, further confirming the lower shrinkage of the latter material.

Low-Shrinkage, Positive-Tone Photoresists. Although various types of 3D photonic structures have been fabricated from polymers, to obtain a PC with a complete PBG, polymeric structures are often used as sacrificial templates for infiltration of a higher index inorganic material. After removal of the polymer template, an inverse inorganic PC is obtained (see later discussion in section 3). Currently most of the 3D polymer microstructures are created in negative-tone photoresists, which form highly cross-linked 3D networks that are difficult to remove by solvent or heat below 400 °C. It will be advantageous to pattern 3D structures in positive-tone resists that can be easily dissolved in an organic solvent after infiltration. In addition, positive-tone photoresists generally possess low or no shrinkage and the solubility in aqueous base developer is attributed to the polarity change before and after exposure to light.[179,180] A handful of groups have used commercially available positive-tone resist, AZ5214 (Clariant International Ltd.), to create 2D and 3D structures.[22,181] AZ5214 is a two-component resist system, a novolac resin as matrix and a diazonaphthoquinone as photoactive component or sensitizer. Upon exposure, the base-insoluble diazonaphthoquinone undergoes photolysis and Wolff rearrangement to form a ketene.[151] In the presence of trace water, the ketene forms a base-soluble indenecarboxylic acid and generates a positive-tone feature. The unexposed regions can be removed with acetone. It seems that positive-tone resists give better contrast and sharper corners than negative-tone resists. However, they are not widely used for PC fabrication due to strong absorption of the aromatic groups in AZ5214 in the UV−vis region and issues such as wettability and dissolution rate of aqueous base in a relatively hydrophobic thick film, therefore limiting the film thickness to less than 5 μm.[181]

Organic−Inorganic Hybrids. As discussed above, a 3D polymer structure can be used as a template for infiltration of a higher refractive index material into the pores to obtain the inverse 3D PC. Backfilling and calcination processes, however, often suffer from volume shrinkage that causes pattern collapse and crack formation, and, more importantly, incomplete filling. An alternative approach is to directly pattern 3D photonic structures from an organic−inorganic hybrid photoresist. Organosilicates have been prepared from 3-methacryloxypropyl trimethoxysilane with water and an acid catalyst through sol−gel reaction.[182,183] The addition of transition metal alkoxide precursors, such as zirconium propoxide and titanium propoxide, to methacrylic acid (MA) produces photo-cross-linkable organic−inorganic composites (also see discussion in section 2.4). Other titanium-containing photoresists have been synthesized from the mixture of titanium ethoxide (TE), methacrylic acid, and ethylene glycol dimethacrylate (EGDMA).[184] The TE and MA produce the titania−acrylate composites while EGDMA acts as a cross-linker. Nevertheless, the increase of refractive index of using hybrid materials is rather limited to less than 2.0.

Another potential advantage of hybrid materials is their high thermal and mechanical robustness. In addition to sol−gel reactions to prepare the hybrid materials, inorganic nanoparticles, such as silica, have been dispersed in the

Scheme 3. Illustration of Photoacid Generation and Crosslinking Reaction in Poly(2-hydroxyethyl methacrylate-*co*-methyl methacrylate). (Reprinted from ref 190. Copyright 2005 Royal Society of Chemistry.)

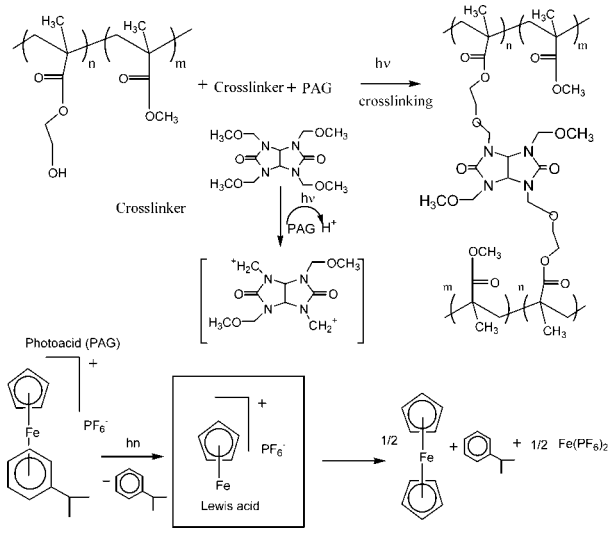

photoresist formation as a reinforcement.[185] However, the high loading of inorganic materials could significantly lower the resist photosensitivity and make the film crack-prone as film thickness increases. The higher refractive index of the resists during 3D fabrication could also cause lattice distortion during the HL fabrication due to a refraction effect at the air−film interface (see earlier discussion on low-shrinkage materials). Moon et al. have investigated the direct fabrication of 3D silica-like structures from epoxy-functionalized cyclohexyl polyhedral oligomeric silsesquioxanes (POSS) using holographic lithography.[186] POSS is a unique class of hybrid materials, which possess the structure of cube-octameric frameworks with eight organic corner groups.[187] It has the chemical composition $RSiO_{1.5}$ with thermal and mechanical properties intermediate between SiO_2 and organic polymers. Unlike SiO_2, each POSS molecule contains nonreactive organic moieties, making it compatible with various polymer systems and enhancing its crack resistance. The 3D epoxy POSS structures were maintained without global volume shrinkage during the heat treatment (up to 400 °C) by thinning the struts that connect motifs. Further, they could be conveniently converted to 3D silica structures, which can be subsequently removed by aqueous hydrofluoric acid (HF) solution at room temperature, thus being suitable for infiltration of a wide range of organic and inorganic materials.

Responsive Materials from Hydrogels. Responsive hydrogels have been widely used as smart materials because they exhibit large volume and shape changes in response to external stimuli, such as pH and temperature, electric potential, chemicals, and biological agents. 3D hydrogels have been fabricated for microfluidic switches and actuators,[188] sensors,[64−66] and cell scaffolds.[189] So far, most of them are fabricated by backfilling a colloidal crystal template with liquid precursors, followed by UV curing through radical polymerization and removal of the template by solvent.[64−66,189] During each of the processing steps, it is possible to introduce additional defects, and template materials suitable for room temperature backfilling and removal without pattern collapse are rather limited.

Direct photopatterning of hydrogels from its liquid monomers or prepolymers using interference lithography methods

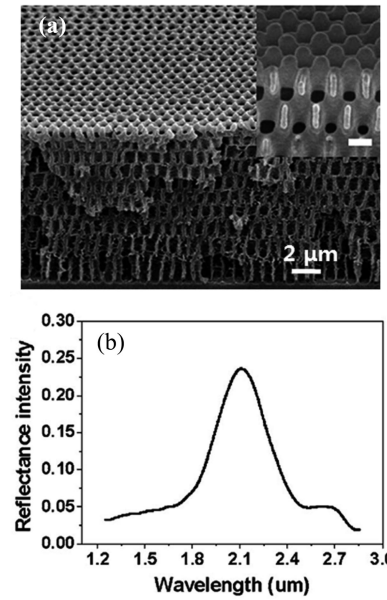

Figure 10. Structure and optical reflectance of 3D hydrogel PCs via holographic lithography. Typical SEM images of (a) tilted cross-section of a fractured sample. The inset shows windows between lattices on the (−110) plane. Scale bar: 500 nm. (b) reflectance spectrum of a nitrogen-dried hydrogel structure measured by Fourier transform IR at room temperature. (Reprinted from ref 68. Copyright 2008 Wiley-VCH Verlag GmbH & Co. KGaA.)

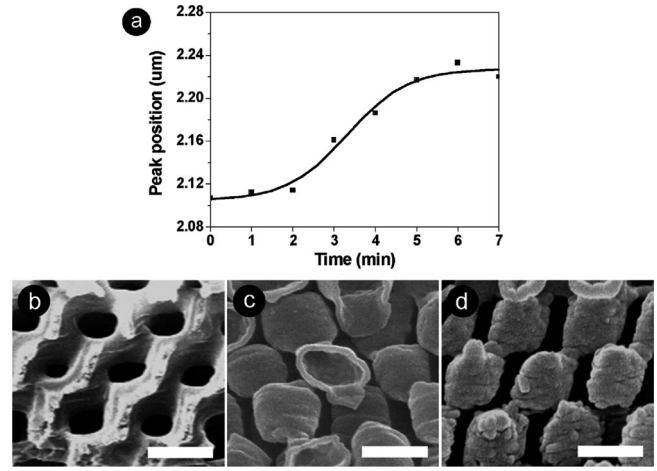

Figure 11. (a) Reflectance peak shift in response to the structural change with time after the dried sample was exposed in the humid air with 100% relative humidity. (b) Cross-sectional SEM images of bare hydrogel PC at the dry state. (c,d) SEM images of inverted silica structures from hydrogel PCs after deposition of silica using dry and swollen hydrogel PCs, respectively. All scale bars are 500 nm. (Reprinted from ref 68. Copyright 2008 Wiley-VCH Verlag GmbH & Co. KGaA.)

is not possible. Photo-cross-linking during exposure will disturb the original interference pattern due to the change of refractive index, and inhomogeneity of radical formation and diffusion in the exposed regions will limit the achievable resolution to a few micrometers. Yang et al. have developed a photosensitive hydrogel precursor, poly(2-hydroxyethyl methacrylate-*co*-methyl methacrylate) (PHEMA-*co*-PMMA), for fabrication of soft, biomimetic microlens arrays.[190] The side chain hydroxyl groups of PHEMA can be cross-linked by photoacid generators (PAG) and external cross-linkers, tetramethoxymethyl glycouluril (TMMGU) (see Scheme 3). The copolymer has a high T_g (≥100 °C); therefore, acid diffusion occurs only at the post-exposure baking (PEB)

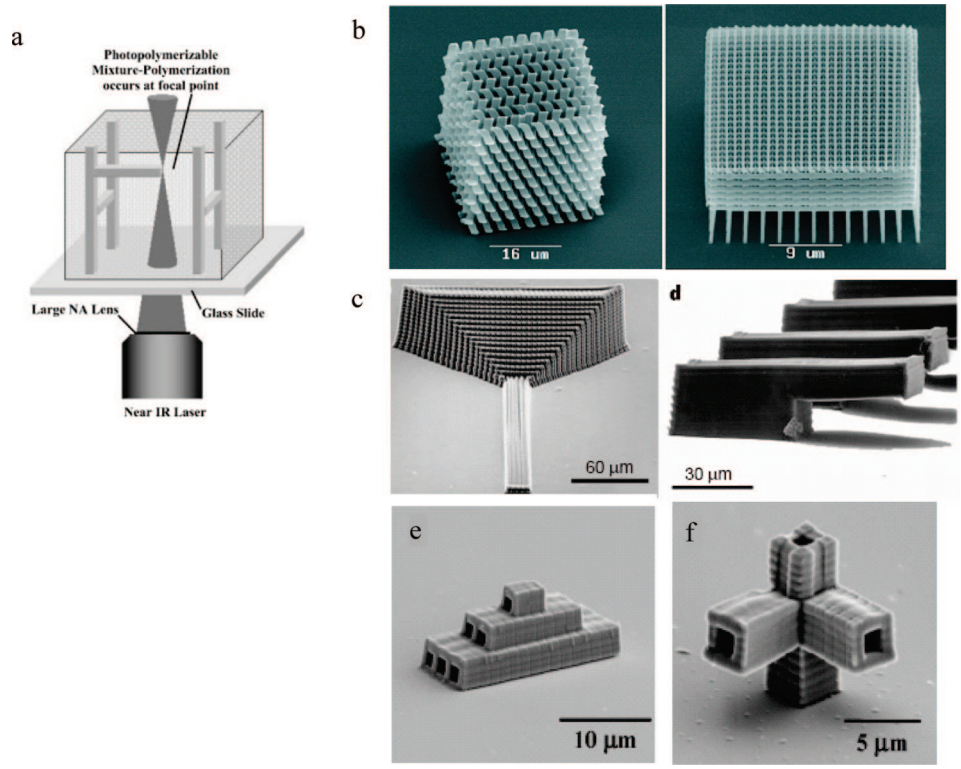

Figure 12. (a) Schematic illustration of two-photon 3D lithography. (Reprinted from ref 35. Copyright 2006 John Wiley & Sons, Ltd.) (b−d) Examples of arbitrarily shaped 3D microstructures fabricated by two-photon lithography: (b) wood-pile photonic band gap structures from zirconium sol−gel material (Reprinted with permission from ref 209. Copyright 2008 American Chemical Society), (c) tapered waveguide structure, and (d) array of cantilevers from triacrylate (Reprinted with permission from ref 33. Copyright 1999 Nature Publishing Group), (e) a stack of microcapillaries of various lengths with inner diameters of <2 μm, and (f) microcapillary intersections from PDMS. (Reprinted from ref 205. Copyright 2004 American Chemical Society.)

stage. PMMA is copolymerized with PHEMA to control the content of hydroxyl groups and avoid physical gelation of PHEMA by itself. The hydroxyl groups will allow for introduction of many types of functional groups (e.g., acrylic acid, glycidylmethacrylate, and acrylamide) in the copolymers to realize different 3D hydrogel structures with tailored architectures, tunability, and functionalities. Based on this photochemistry, Kang et al. fabricated 3D thermoresponsive hydrogel PCs using prism holographic lithography.[68] Figure 10 shows typical scanning electron microscopy (SEM) images and reflection spectra of 3D hydrogel PCs, respectively. The spacing between motifs and the lattice spacing are around 680 and 770 nm, respectively. Within 10 min exposure to humid air (100% relative humidity), the reflectance peak was red-shifted from 2.10 to 2.22 μm (Figure 11a) due to swelling of the hydrogel network by water. The structural change in the course of swelling was captured by chemical vapor deposition (CVD) of silica on the hydrogel surface (see Figure 11b−d). The lattice spacing from the inverted silica structure (or swollen hydrogel) was elongated in the [111] direction by 10% relative to that from the dried hydrogel, while the lateral dimensions remained unchanged due to the pinning of the structure at the substrate. The swollen hydrogel PCs exhibited thermoresponsive behavior, which could be explained by the lowered T_g during swelling. Therefore, the hydrogel network deforms in response to the temperature change, where the connecting bridges between the motifs are collapsed in order to lower the surface energy. Such deformation is reversible below 50 °C, which can be attributed to the elasticity of cross-linked hydrogels.

Later, Jang et al. adapted the above chemistry to synthesize a photopatternable random terpolymer of poly(hydroxyethyl methacrylate-*ran*-methyl methacrylate-*ran*-methacrylic acid), poly(HEMA-*r*-MMA-*r*-MAA). Using PMIL, they fabricated 3D networks as a new platform for biomedical applications.[69] The fully open 3D hydrogel/air networks were demonstrated as a pH-responsive polymeric drug-release system for the delivery of neurotrophins to enhance the performance of neural prosthetic devices. Additionally, the open hydrogel structure could provide direct access of neuronal growth to the device for improved electrical coupling.

2.4. Two-Photon Lithography (TPL)

Although interference lithography has been shown as a promising method to photopattern 1D, 2D, and 3D periodic photonic structures with submicrometer periodicity over a large area, it is not suitable to fabricate arbitrary structures, such as cavity defects and waveguide structures, for device functions. In contrast, two-photon lithography is well suited for constructing arbitrarily shaped 3D structures.[33−37]

By tightly focusing a femtosecond near-IR laser beam (typically from a Ti:sapphire pulse laser) into the resin, subsequent photoinduced reactions, such as polymerization of triacrylates,[33,191] SU-8,[34,192,193] and deprotection of poly(methacrylates),[179] occur only in the vicinity of the focal point, allowing direct writing of 3D complex patterns by scanning the sample on motorized stages (Figure 12).

In the case of TPP of acrylates, viscous liquid resins become solidified in the exposed region, analogous to a negative-tone lithographic process. The desired 3D structure is fabricated via two-photon absorption and subsequent photopolymerization, followed by removal of the unreacted liquid resin by a solvent. In two-photon absorption (TPA),

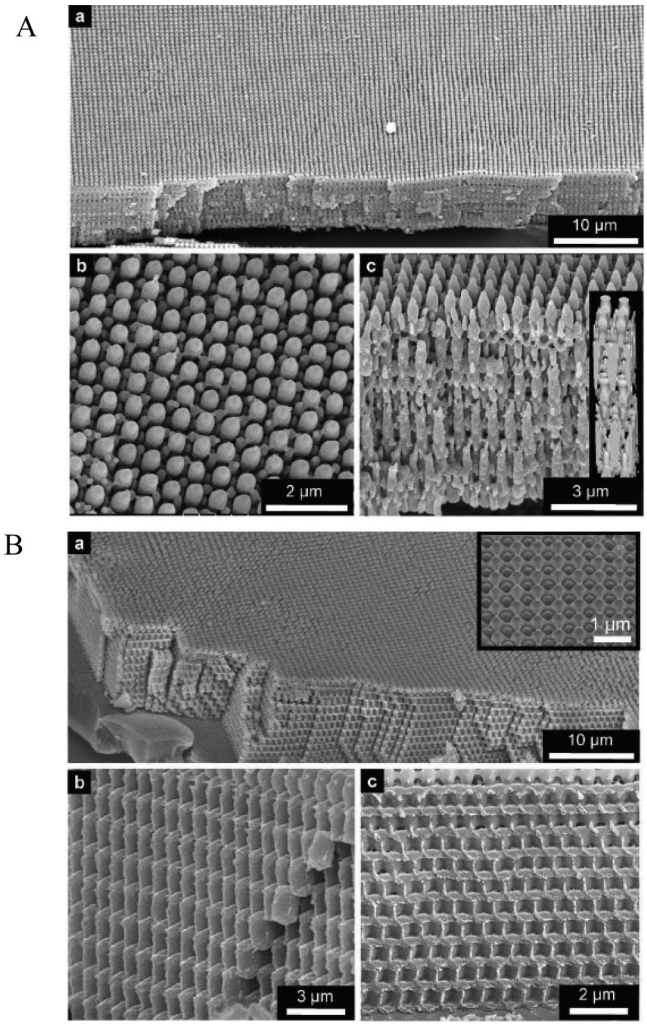

Figure 13. SEM images and modeling of 3D structures made through (A) a one photon process and (B) a two photon process with mask 1(square array of circular dots, $d = 570$ nm, $h = 510$ nm, $p = 710$ nm). (A) (a) Large area angled view, (b) top view, (c) cross-sectional view and modeling (inset). (B) (a) Large area angled view and top view (inset), (b and c) cross-sectional views at different angles. (Reprinted from ref 195. Copyright 2006 Optical Society of America.)

changes of the physical or chemical properties of the resin are quadratically dependent on the intensity of the laser beam,[194] such that the rate at which two-photon dye molecules are excited decreases rapidly (as z^{-4}) with the distance from the focus and the excitation is confined in a small volume around the focus (on the order of λ^3, where λ is the wavelength of the incident beam). Therefore, two-photon lithography not only allows for fabrication of structures that are difficult to access by conventional single-photon processes but also offers greater spatial resolution than other 3D microfabrication techniques by far.[34,191] By taking advantage of such a quadratic dependence of TPA probability on the photon fluence density and radical scavenger from dissolved oxygen molecules near the focal volume, Kawata et al. demonstrated a subdiffraction-limit spatial resolution of 120 nm using a Ti:sapphire laser ($\lambda =$ 780 nm).[34] Haske et al., on the other hand, produced nanoscale features as small as 65 ± 5 nm reproducibly by using 520 nm femtosecond pulsed excitation of a 4,4′ bis(di-*n*-butylamino)biphenyl chromophore to initiate cross-linking in a triacrylate blend.[191]

Recently, Jeon et al. has explored the combination of two-photon absorption with PMIL to fabricate a wider range of 3D structures with variable geometries.[195] In PMIL, passage of unfocused laser pulses through transparent phase masks generates complex but well-defined 3D distributions of intensity near the surfaces of the masks. Using the same mask, the SU-8 films were exposed to UV and near IR light for one-photon and two-photon lithography, respectively. It was found that the dominant in-plane periodicities of the one- and two-photon structures were similar except that the depth variations of the geometries were quite different due to the different intensity distributions of the light within the polymer film. Figure 13 shows 3D structures of SU-8 fabricated from one photon ($\lambda = 355$ nm) and two photon ($\lambda = 810$ nm), respectively, together with a phase mask ($d = 570$ nm, $h =$ 510 nm, $p = 710$ nm, circular dots in square array). As seen in Figure 13B, the two photon process produced a simple body centered tetragonal (bct) structure, with geometries close to fcc, and the lattice parameters of $a = 710$ nm and $b = 1780$ nm.

2.4.1. Two-Photon Photoinitiators

Successful structuring by TPA with high resolution is critically dependent on the sensitivity of the two-photon initiators at the processing wavelength. A low aspect ratio of a voxel (volumetric pixel) at the focal point will allow for layer-by-layer fabrication of 3D microstructures using TPP.[36] To achieve a high spatial resolution and minimize the aspect ratio of voxels, it is necessary to keep the low laser power and short exposure time near the threshold energy, therefore reducing focal spot duplication and voxel growth. Commercially available PIs (typically single-photon UV initiators) often show low activity. Highly efficient TP photoinitiators (PIs) that exhibit larger TPA cross sections, δ, have been synthesized for 3D fabrication.[33,179,191,196−200] Planar chromophores with extended π-system and donor (D) and acceptor (A) groups, D-π-D, D-π-A-π-D, and A-π-D-π-A (where π is a π-conjugated bridge), have been shown with large δ relative to the parent unsubstituted conjugated molecules.[33] A series of bis dialkylamino- or diarylamino-substituted diphenylpolyenes and bis(styryl)benzenes have been investigated.[196] The type and length of the conjugated chain and the position of dialkylamino or diarylamino substitution play a role in the magnitude of the peak two-photon absorptivity. Increasing the length of the conjugated linker in D-π-D molecules, through use of diphenylpolyene or phenylene-vinylene-type bridges, also results in increased δ. This increase is essentially linear with chain length but depends on the type of bridge, with the phenylene-vinylenes showing the larger increase. Likewise, derivatives of single photon PI, 1,5-diphenylpenta-1,4-diyne-3-one (DPD), with auxochromic groups (−OMe, −SMe, $-NMe_2$, and $-NPh_2$) were synthesized to shift the absorption from ultraviolet−visible (UV−vis) into the visible range of the spectrum. By para-substitution of the benzo-aromatic moiety with different auxochromes such as a methoxy-group (O-DPD), a thiomethyl-group (S-DPD), or a dimethylamino-group (N-DPD), a red-shift in the absorption spectrum to the visible region was observed. Compared to single-photon initiators, N-DPD offered outstanding performance in patterning PDMS at ~800 nm, while the PI content was a factor of 100 lower.[200] As shown in Figure 14,[36] these chromophores can be classified into three groups according to their π-centers: (i) fluorene derivatives (Ia−Ib), (ii) dithieno[3,2-*b*;20,30-

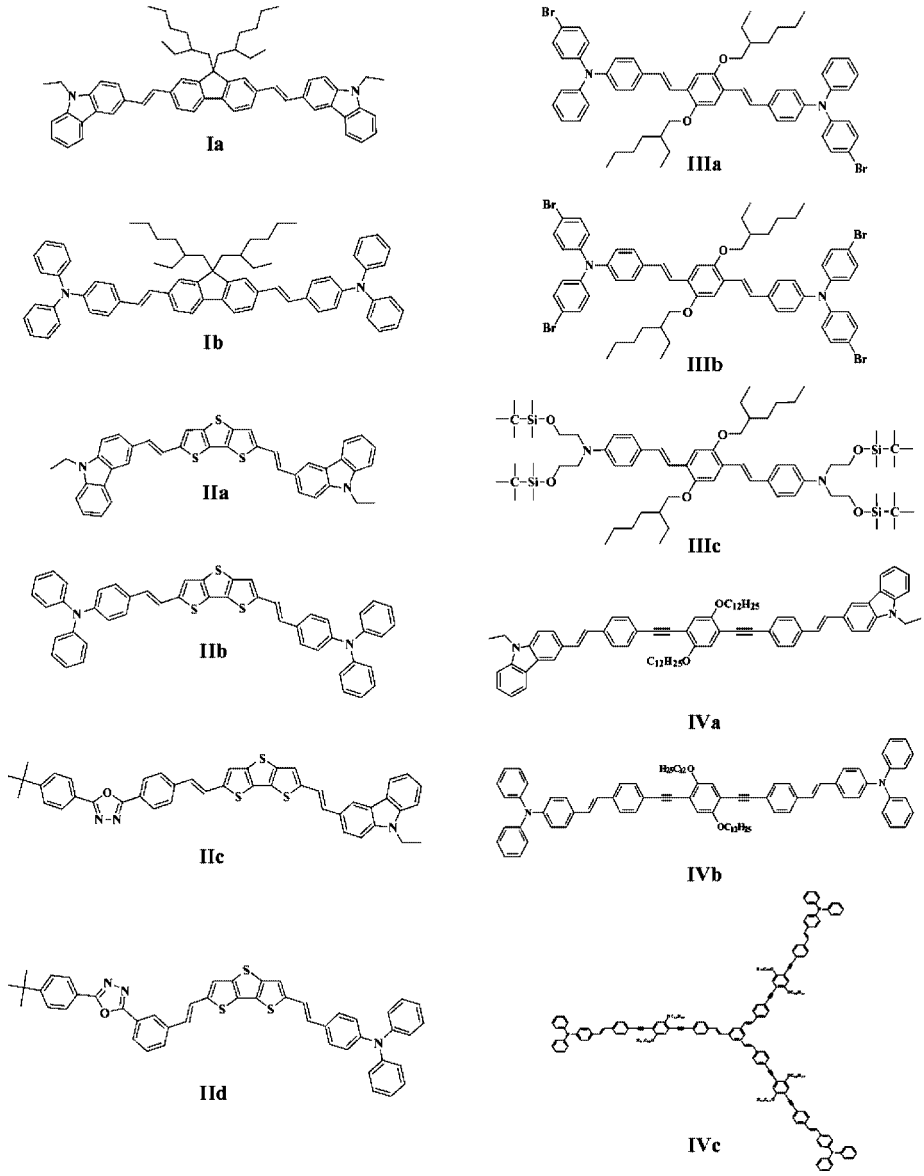

Figure 14. Molecular structures of two-photon absorbing materials. (Reprinted from ref 36. Copyright 2006 John Wiley & Sons, Ltd.)

d]thiophene (DTT) derivatives (IIa−IId), and (iii) phenylenevinylene derivatives (IIIa−IIIc) and phenyleneethynylene derivatives (IVa−IVc).

2.4.2. Photosensitive Materials Used in Two-Photon Lithography

To date, many of the 3D microstructures fabricated by two-photon lithography have been based on radical-initiated polymerization of multifunctional (meth)acrylates partly due to the readily available monomers (see Figure 15a) and tertiary amines for electron transfer to generate radicals upon two-photon excitation.[33,201] Owing to the insensitivity of environmental oxygen, a radical scavenger, and high T_g of SU-8 (Figure 15b), photoinitiated cationic polymerization of epoxides has received increasing attention in TPP for fabrication of robust 3D PCs, typically from commercially available photoresist SU-8 (MicroChem) consisting of a one-photon UV photoinitiator (mixed triarylsulphonium/hexafluoroantimonate salt in propylene carbonate solvent).[34,192,193,202,203] However, traditional one-photon UV-sensitive PAGs have very low two-photon sensitivity; therefore, the working window to direct write 3D structures by TPP could be narrow. Highly sensitive photoacid generators were synthesized by covalently attaching sulfonium moieties to the two-photon chromophore to fabricate 3D photonic structures via photoacids and the chemical amplification mechanism.[179] Recently nonionic PAGs have been synthesized,[204] of which a chromophore and a photocleavable group are covalently linked by a flexible joint, thus allowing for microfabrication of 3D structures via both radical and cationic polymerization mechanisms under one- and two-photon excitation conditions.

Photocurable PDMS System. Besides applications in photonics, TPP has been used to fabricate microelectromechanical systems (MEMS), microfluidics, tissue scaffolds, and biomedical devices. To this end, poly(dimethylsiloxane) (PDMS)-based microstructures have been fabricated by TPP via photohydrosilylation and radical-initiated cross-linking of a viscous liquid composed primarily of dimethylvinyl-terminated PDMS, poly(methylhydrosiloxane-*co*-dimethylsiloxane), such as Sylgard 184 (Dow Corning), which is biocompatible and has been widely used in soft lithography and microfluidic channels (see Figure 15c).[200,205] In addition, the elastomeric nature of PDMS makes it deformable in organic solvent and/or under mechanical stretching; therefore,

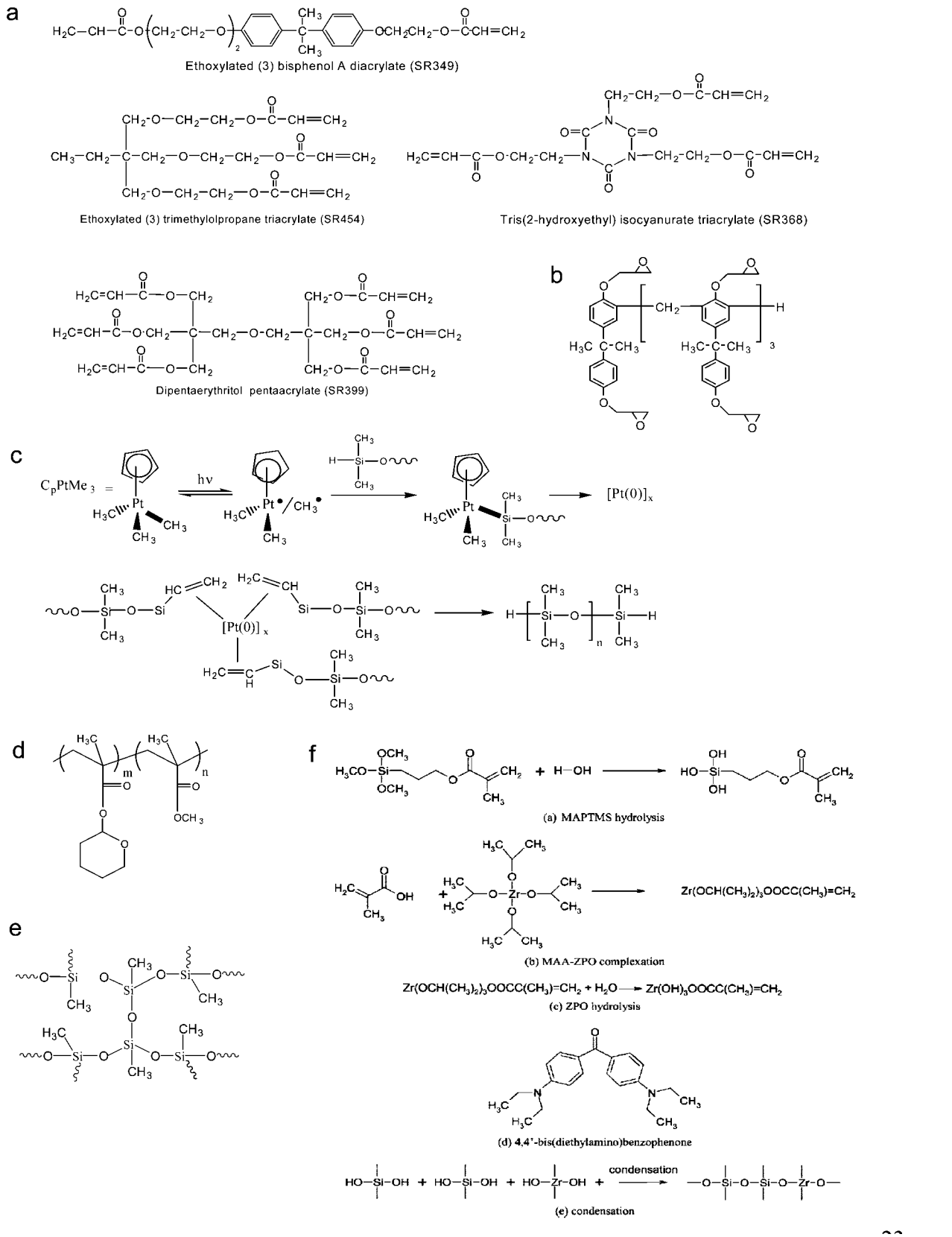

Figure 15. Chemical structures of monomers and polymers used in two-photon lithography and related chemical reactions: (a) multifunctional acrylates; (b) SU-8; (c) illustration of photohydrosilylation of dimethylvinyl-terminated PDMS, poly(methylhydrosiloxane-*co*-dimethylsiloxane), via platinum catalyst, (η5-cyclopentadienyl)trialkylplatinum; (d) positive-tone resist, PTHPMA-PMMA; (e) methyl silsesquioxane (MSQ); (f) synthesis of low-shrinkage, photosensitive, zirconium sol−gel material. (Reprinted from ref 209. Copyright 2008.)

3D PDMS structures are of interest as tunable photonic[101] or phononic crystals.[181]

Positive-Tone Resists. As discussed earlier in section 2.3.3, chemically amplified positive-tone photoresists can be particularly useful for fabrication of high fidelity 3D structures. In comparison to acrylate based materials, positive-tone resists (typically methacrylate based polymers) exhibit much lower shrinkage and can be readily removed

using organic solvent at room temperature. A random copolymer of tetrahydropyranyl methacrylate (THPMA) and methyl methacrylate (MMA), with or without *tert*-butyl methacrylate (tBMA), was synthesized.[180] MMA was chosen to provide mechanical strength and optical transparency, THPMA and *t*BMA were to offer solubility change upon photoacid catalyzed deprotection reactions, converting THP and/or *tert*-butyl ester groups to carboxylic acid groups, therefore rendering the exposed regions soluble in an aqueous base developer. Cleavage of THP ester linkages requires much lower activation energy than that of *tert*-butyl ester linkages; therefore, resists containing THPMA will be more desirable in thick film fabrication. However, such resists could also undergo "dark reaction" to cleave the ester linkage at room temperature. To increase shelf life, copolymerization of high activation energy *t*BMA or addition of base in the system to suppress the "dark reaction" is a common practice.

Photosensitive Hybrid Materials. Another class of material of interest in direct laser writing by TPP is inorganic−organic hybrids, such as ORMOCERs.[206] Typically, the hybrid precursors are prepared in two steps: first, an inorganic−organic sol with photopatternable organic moieties, including (oligo-) methacryl, styryl, and epoxy groups, is synthesized by hydrolysis/polycondensation reactions, followed by partial cross-linking of the polycondensed alkoxysilanes. The sol−gel becomes solidified and patterned upon exposure to a femtosecond pulse laser, whereas the unexposed regions will be removed using an organic solvent as developer. Their physical and chemical properties can be tailored by the organic moiety, the organic/inorganic ratio, and the structure of the resulting sol−gel precursor. For example, refractive indices can be varied in the range between 1.44 and 1.56. The Young modulus and, thus, the mechanical and thermal stability can be increased by increasing the amount of inorganics. As a result, the coefficient of thermal expansion (CTE) and the optical losses in the NIR regime are reduced. For most hybrids, however, their organic components decompose at relatively low temperatures (<300 °C).

Recently, Jun et al. have synthesized methylsilsequioxane ($CH_3SiO_{1.5}$, MSQ, Figure 15e) precursors with a ladder structure for direct laser writing (DLW) woodpile 3D PCs using TPP.[207] This photoresist has the lowest amount of organic groups, resulting in high thermal stability. The decomposition of methyl groups starts at ca. 590 °C in nitrogen and ca. 430 °C in air, making the MSQ 3D structures compatible with typical silicon infiltration steps, such as low-pressure chemical vapor deposition (LPCVD) using silane at 500−550 °C. The silsesquioxane-based photoresist chemistry was recently modified and applied to conformal phase mask interference lithography to create 3D periodic inorganic microstructures.[208]

Nevertheless, structures fabricated via photopolymerization of viscous liquids often suffer large shrinkage, leading to structure distortion and raising questions about structure stability and reproducibility. From a copolymer of methacryloxypropyl trimethoxysilane (MAPTMS) and zirconium *n*-propoxide (ZPO) (see Figure 15f), Ovsianikov et al. investigated fabrication of 3D PCs by TPP.[209] By organically modifying ZPO only partially (up to 30 mol %), they fabricated ultralow shrinkage woodpile PCs with good resolution (3.6 μm long free-hanging lines and a structure period of 1.2 μm). In addition, the addition of ZPO significantly increases the photosensitivity of the photopolymer. A clear band-stop in the near-IR region was observed. The low shrinkage was attributed to the double polymerization ability of sol−gels.[210] During the pre-exposure baking, the film underwent preshinkage through condensation of the alkoxy groups, releasing alcohol, water, and any other solvents present in the film, to form an inorganic matrix. In the subsequent TPP, an organic network was formed without the release of any small molecules; volume reduction was found directly related to the average irradiation dosage. When well above the polymerization threshold, the 3D structures exhibited very low shrinkage.

Chalcogenide Glasses. Wong et al. explored the possibility to directly write a high-refractive-index woodpile PC in As_2S_3 chalcogenide glasses.[211] As_2S_3 is an amorphous semiconductor material with high refractive index (n = 2.45−2.53) and is highly transparent throughout the near-IR and IR spectral regions. Chalcogenide glasses are known for their photoinduced metastabilities.[212] They have been used widely in optical storage media. First, As_2S_3 was thermally evaporated on a substrate, mainly composed of As_4S_6 cage molecules. Under local photoexposure, the As_4S_6 cage molecules are polymerized, forming a cross-linked As_2S_3 glassy network. This allows for selective wet etching of As_4S_6 cage molecules in the unexposed regions by a mixture of a secondary amine (e.g., diisopentylamine) and a polar solvent (e.g., dimethylsulfoxide). Neither shrinkage nor expansion of the written structure was observed. The fabricated woodpile structure exhibited a complete gap of 3.5% in the IR. The direct fabrication of high-refractive-index PCs is advantageous, since it eliminates the need for subsequent inversion, which will be discussed in detail in the following section. Larger PBGs could be achieved when higher refractive index chalcogenide glasses, such as As_2Se_3 (n = 2.78) or As−Se−Te composites (n up to 3.2), are used for 3D patterning.

2.4.3. Introducing Controlled Defects in Photonic Crystals

Although a wide range of 3D micro- and nano-objects have been fabricated using two-photon lithography, the serial writing nature of this method leads to relatively slow patterning throughput compared to the aforementioned interference lithography. Therefore, it is often attractive to create defect structures in 3D PCs fabricated by other techniques, for example, holographic lithography[213−215] and colloidal assembly.[201,216−218] Incorporation of controlled defects is the precondition for manipulating photons in PCs. There have been two recent reviews detailing the efforts taken to this end.[216,217]

Lee et al. first reported on writing defect structures in colloidal crystals using a tightly focused multiphoton laser beam.[201] Typically, photo-cross-linkable resins are infiltrated in colloidal PCs or their inverted structures, followed by two-photon polymerization to write the defects (or waveguide structures).[115,215,218] In the post-fabrication process, precise registration between the embedded defect structures and the surrounding 3D lattice is critical to obtain low-loss high quality waveguides. However, in the past the low resolution of the reflectance imaging from the monomer/colloid interface has limited the degree of control on the registration. By switching from a reflective to a fluorescent imaging technique, Nelson et al.[219] recently have demonstrated the possibility to achieve concurrent high resolution imaging and

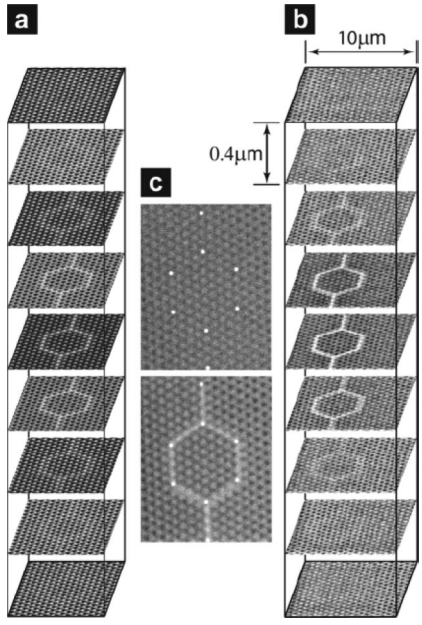

Figure 16. Latent images of a waveguide in a holographic pattern created by sequential holographic and scanning two-photon optical exposure. (a) The target structure: the sum of the calculated photoacid densities created in the two-step exposure process. (b) Experimentally measured photoacid density: confocal sections are recorded at 0.4 lm intervals. (c) Confocal section (top) recorded after holographic exposure and used to align the waveguide-writing step and the corresponding section (bottom) after waveguide writing. The overlay of white dots indicates reference points used to align the test device. (Reprinted from ref 214. Copyright 2006 Wiley-VCH Verlag GmbH & Co. KGaA.)

feature writing during TPP, enabling excellent lattice registration and exact placement of defect features in colloidal crystals.

TPP has also been applied to holographic lithography patterns. In this case, it is not necessary to infiltrate photopolymerizable resin after HL since the photoresist system can be formulated to be sensitive to both visible light and two-photon excitation in IR. For example, by adding pH-sensitive dye coumarin 6 in conventional SU-8 photoresists to visualize the photoacid distribution under a florescence microscope, Scrimgeour et al.[214] have patterned a 3D structure by HL, immediately followed by defect-writing using TPP before subjecting the pattern to PEB and developing steps. Here, the coumarin 6 can be protonated by the released photoacids, resulting in a red-shift of adsorption in the spectra. As seen in Figure 16, excellent registration between the defect and the underlying HL 3D pattern has been achieved, and the lateral resolution of two-photon writing was clearly good enough to restrict the defect to one motif of the 3D structures.

3. Backfilling Chemistry

Although major progress has been made in developing fabrication methods to create a wide range of 3D photonic structures, the low refractive index of the patterned films ($n < 1.7$) has become the bottleneck that limits the realization of complete PBGs in the fabricated 3D crystals for device applications. The minimum required refractive index contrast to open a band gap is 1.8 for a diamond D structure.[39] Many research groups have investigated the backfilling strategy to create high-refractive-index PCs from inorganic materials, including titania ($n = 2.2-3.0$),[16,143,220] selenium ($n = 2.5$),[123] cadmium−selenium ($n = 2.5-2.75$),[221] amorphous silicon ($n = 3.45-4.2$),[10,154,215,218,222−226] germanium ($n = 4.0$),[227−229] and Si/Ge multilayer shells[230] using the fabricated 3D structures as templates. These inorganic materials can be deposited through either a dry process, including chemical vapor deposition (CVD),[10,154,215,218,222−228,230] atomic layer deposition (ALD),[231−235] and melting,[123] or wet chemical methods, including liquid phase sol−gel reaction,[16,143,236−238] electrochemical reaction,[221,239] and precipitation.[240,241] The template is subsequently removed by solvent, thermal decomposition, or selective chemical etching to backfill high refractive index PCs with the inverse structure.

Most templates studied so far for backfilling are from closely packed colloidal crystals, which have been reviewed by several groups on choice of materials, the backfilling morphologies, and PBG properties.[242−247] Figure 17 illustrates several possible backfilling morphologies in inverse opals, including residual volume structures (RVS), shell structures (ShS), and skeleton structures (SkS).[248] The RVS and ShS show a complete filling of residual volume and conformal coating, respectively. The SkS consists of cylinders connecting crossings in octahedral and tetrahedral voids of the opal. Theory has shown that the inverted fcc structures can possess a complete PBG between the eighth and the ninth bands, with 4.25 and 7.35% from high-refractive-index Si and Ge, respectively.[249] In the case of skeleton structures, theoretical calculation has suggested a larger PBG at the eighth or ninth band over shell structures and the appearance of an additional PBG at the fifth or sixth band.[237] Nevertheless, it seems that the morphology of backfilled inorganics does not have a large effect on PBG width but can tune the band gap position within <200 nm wavelength.[250]

In comparison, 3D lithography approaches are more versatile to create a wide range of lattices. For example, various triply periodic cubic phases, including simple cubic P, gyroid G, and diamond D, can be formed by holographic lithography[20,39] and are of particular interest because they possess wide complete PBGs. It has been calculated that the minimum required refractive index contrast is 2.8 for P, 1.9 for G, and 1.8 for D, respectively.[39] Compared to the colloidal crystals, the volume fraction of air cavities can be conveniently controlled by the exposure intensity or the degree of polymerization in a 3D lithography process. However, the 3D structures often possess a narrow pore connection, making it challenging to completely fill the pores. In the case of triply periodic bicontinuous structures, the pore sizes are not uniform within the structure, where the motifs at the lattice points of the corresponding structure are connected by bridges to their nearest neighbors. As the inorganic layer grows conformally and continuously over the template surface, typically in the dry process of backfilling, the surface of the pore network pinches off (i.e., disconnects) at the narrowest pore channels before the interstitial voids are completely filled (see Figure 18), resulting in the loss of PBGs.[154,233] Theoretical simulation of conformal coating on P, G, and D templates suggests that the practically achievable filling fractions at the pinch-off are 84% for D, 98% for G, and 54% for P templates, respectively, resulting in 77% for D and 98% for G of the corresponding maximum PBGs, respectively, and the band gap does not open for P at the pinch-off filling fraction.[251] The study further suggested that the band gap frequencies are not very sensitive to the subtle morphology difference of the deposited layer.

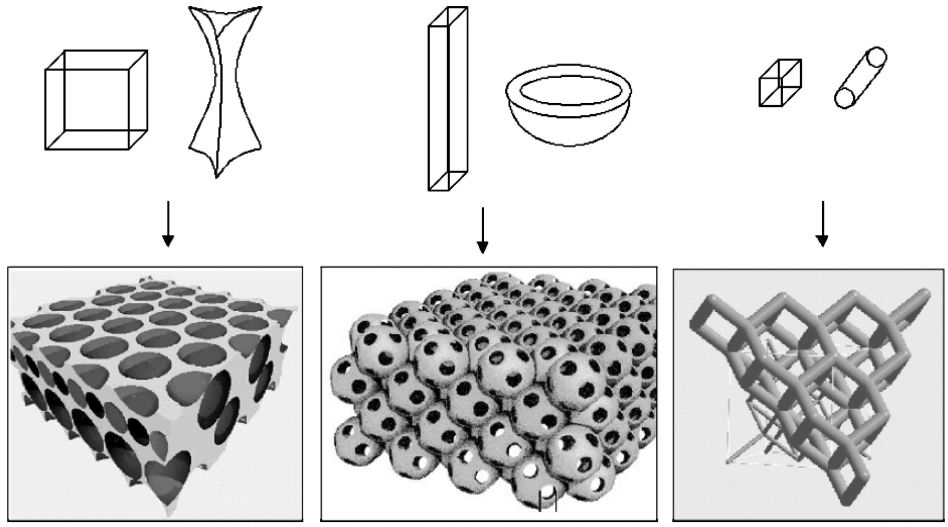

Figure 17. Schematic illustration of the building block concept to produce inverse opals. Three resulting structures with a fcc lattice are residual volume structures (RVS), shell structures (ShS), and skeleton structures (SkS), from left to right. (Reprinted from ref 248. Copyright 2003 Wiley-VCH Verlag GmbH & Co. KGaA.)

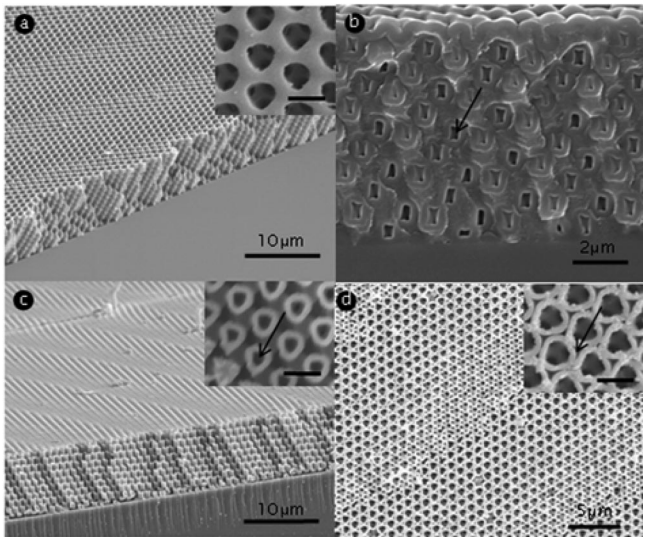

Figure 18. SEM images of diamond-like SU-8 structures (a) and the inverted silica replica before (b) and after (c) the removal of the template. The insets in parts a and c show the (111) plane. Scale bar: 1 μm. The arrows in parts b and c indicate the unfilled air voids. (Reprinted from ref 154. Copyright 2006 Optical Society of America.)

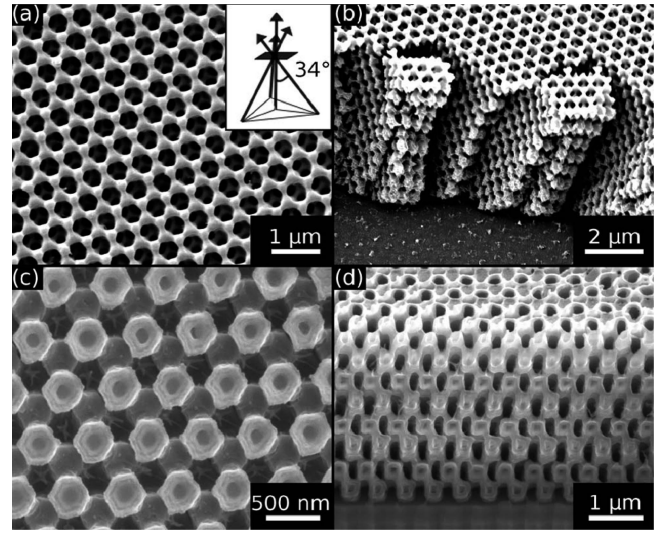

Figure 19. SEM images of the (a) top view and (b) cross section of polymer−air photonic crystals fabricated by holographic lithography with an umbrella beam geometry. SEM images of (c) top view and (d) SEM cross section images of air−silicon photonic crystals from polymer templates. (Reprinted from ref 215. Copyright 2008 American Institute of Physics.)

3.1. Chemical Vapor Deposition (CVD)

Of many high-refractive-index materials, silicon receives the most attention because of its high refractive index (n = 3.5−3.9), transparency in the near-IR and IR regions, and compatibility with existing Si technology. Silicon PCs can provide extreme confinement of light at the diffraction limit and a possible way to manipulate light in micro-optical circuits at telecommunication wavelength. Low pressure CVD (LPCVD) using disilane (Si_2H_6) as precursor has been widely used to deposit silicon (hydrogenated, amorphous) onto colloidal crystals[218,223−226] and holographic[154,215] and two-photon lithography structures.[207]

Since the thermal decomposition of disilane requires high temperature (above 300 °C), at which the polymer templates begin to decompose as well, a double templating method is employed using a sequential SiO_2/Si CVD.[226,252] First, the polymer photonic structure is converted to a silica inverse structure through consecutive exposures to $SiCl_4$ vapor and water vapor using atmospheric pressure at room temperature.[252] Alternatively, a combination of Al_2O_3/SiO_2 bilayer coating was also investigated before subsequent deposition of high-refractive-index inorganic materials (e.g., Ge).[229] A 20 nm Al_2O_3 layer was first deposited on the polymer scaffold by an ALD process at 180 °C, followed by CVD of SiO_2 from $SiCl_4$(g). The Al_2O_3 layer offers higher mechanical and thermal stability than the SiO_2 layer obtained by using CVD, therefore enhancing the stability of the deposited SiO_2 layer and preventing crack formation during subsequent processing steps. Taking this knowledge, Ramanan et al.[215] have attempted a single inversion procedure to convert HL patterned SU-8 3D structures to silicon−air structures by depositing a 30 nm conformal layer of alumina at 90 °C by ALD, followed by LPCVD of disilane at 325 °C for 15 h (see Figure 19). The Al_2O_3 thin layer acted as a sacrificial layer, which was later removed by HF, thus exposing the polymer network to air. This strategy was found

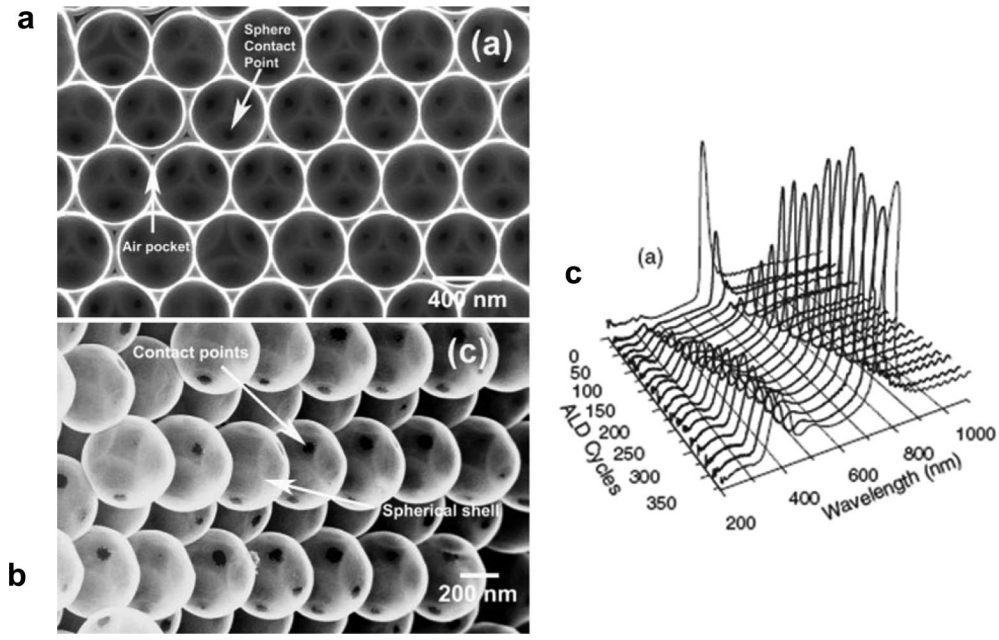

Figure 20. SEM images of titania inverse opal fabricated by a low-temperature ALD process: (a) ion-milled (111) surface; (b) fracture surface; (c) reflectivity data from stepwise TiO_2-infiltrated SiO_2 opal. Measured spectra versus ALD cycles. (Reprinted from ref 231. Copyright 2005 Wiley-VCH Verlag GmbH & Co. KGaA.)

useful to limit crack formation when calcinating the SU-8 template at 410 °C for 4 h.

Recently, laser-assisted CVD has been applied to deposit silicon on silica colloidal crystals.[253,254] A continuous wave Nd:YAG laser (1064 nm wavelength)[253] or a continuous-wave CO_2 laser (10.6 μm wavelength)[254] was used to deposit silicon shells by thermally decomposing disilane gas. By removing the silica particles enclosed in the silicon shells using hydrofluoric acid, hollow spherical silicon-shell arrays[253] and silica-core−silicon-shell[254] PBG structures were produced. By adjusting the silica particle size and Si-shell thickness using different LCVD parameters, this technique is capable of fabricating structures with various morphologies, therefore, will enable engineering the position and width of PBGs.

3.2. Atomic Layer Deposition (ALD)

ALD is an improved version of the CVD process, allowing more uniform conformal coating at a very slow deposition rate. Typically, a binary reaction is split into two half reactions. The growth of inorganic materials in ALD is achieved layer-by-layer through sequential exposure to one of two complementary chemical species, where individual precursors are supplied to the reactor one at a time, coupled with substrate temperature optimization.[255] Therefore, one distinctive characteristic of ALD over CVD is the self-limiting film growth, which enables accurate film thickness control, uniformity over large areas, and good conformity and reproducibility. Various materials, including SiO_2, WN, TiO_2,[231,233,234] ZnS:Mn,[232] TaN_5, GaAs, and Al_2O_3,[229] have been deposited onto a sacrificial template to create high-refractive-index PCs. For example, King et al. fabricated TiO_2 inverse opals by a low-temperature ALD process (Figure 20a,b).[231] The ALD growth was performed by alternating pulses of $TiCl_4$ and H_2O precursors. The reflectivity from the Γ−L direction was measured after each step and demonstrated high precision infiltration of TiO_2 (<1 nm) through ALD (Figure 20c). At a growth rate of 0.51 Å per cycle at 100 °C, maximum infiltration (88%) was achieved by the 350th ALD cycle. Later, the same ALD chemistry was applied onto the holographically patterned SU-8 templates, followed by the reactive ion etching to remove the polymer.[233] Although the growth rate could be further increased by optimizing the ALD conditions, in general ALD is a very slow process.

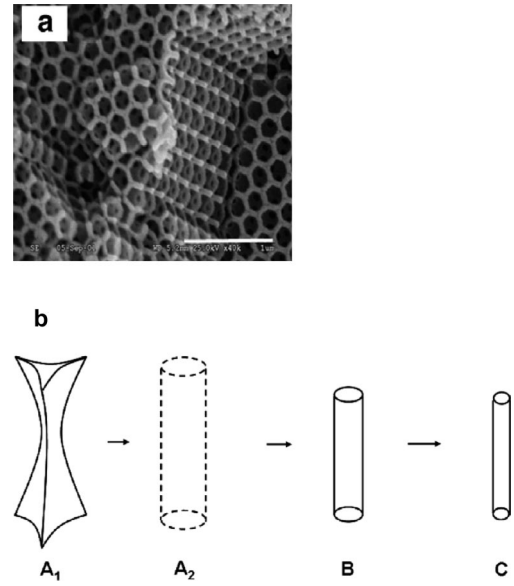

Figure 21. (a) SEM image of titania skeleton structures. (b) Schematic representation of the hypothetical processes during calcination. (Reprinted from ref 250. Copyright 2007 Elsevier.)

3.3. Sol−Gel Reactions

In contrast to dry deposition approaches, wet chemical methods offer greater potential to achieve maximal filling of inorganic materials in the 3D templates.[239,241,256,257] Moreover, Dong et al. discovered a new skeleton morphology when filling the colloidal crystal template with concentrated titania precursor in ethanol solution. The skeleton structure possessed a larger PBG between the eighth and ninth band

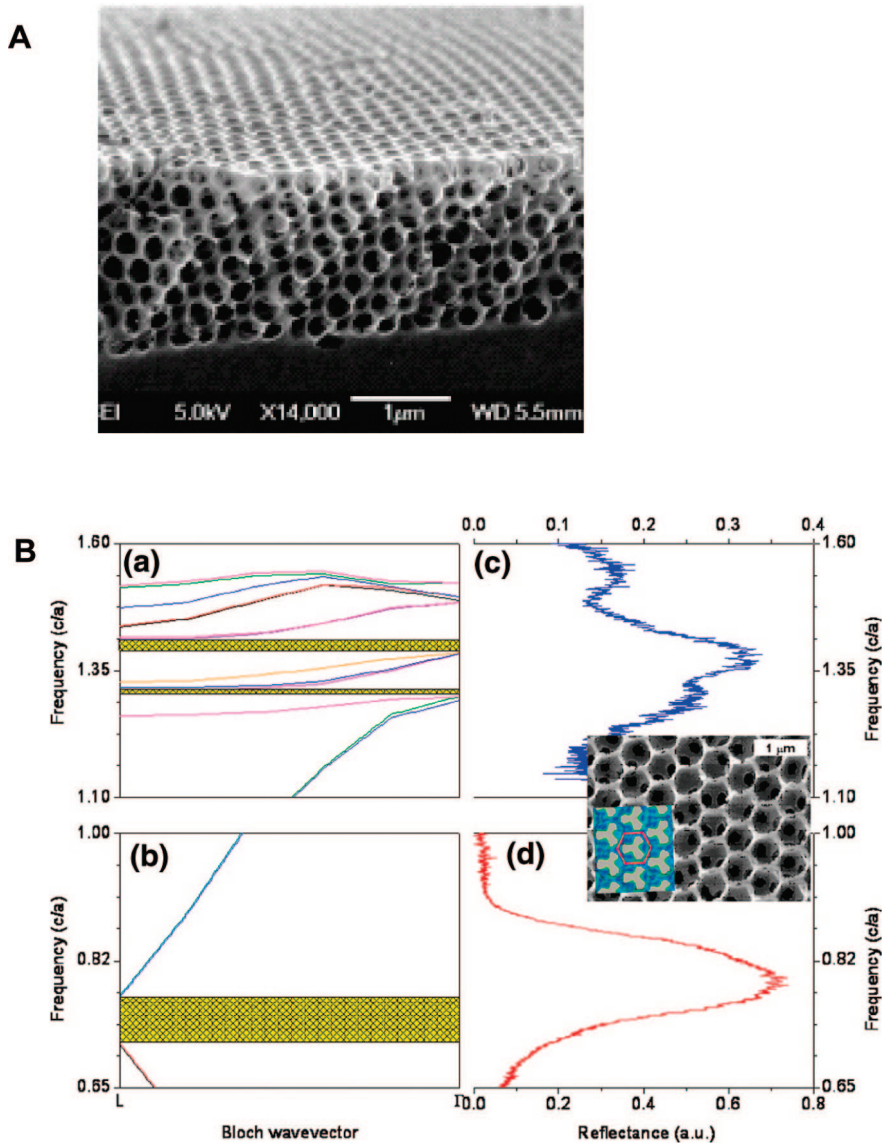

Figure 22. (A) SEM image of titania inverse opals. (B) (a) Calculated high-frequency and (b) low-frequency band structure diagram showing the Γ−L [111] direction for an inverse opal. Stop gaps are indicated by the hatched regions. Optical reflectance spectra of titania inverse opal with lattice constants of (c) 535 nm and (d) 310 nm. Inset: SEM titania inverse opal. (Reprinted from ref 238. Copyright 2008 American Chemical Society.)

over shell structures, and an additional band gap between the fifth and sixth band.[236,237] They assumed that the obtained skeletons were snapshots on the synthesis pathway from a titania gel to a solid structure during the heat treatment.[250] Briefly, during calcination removal of the PS colloidal template concurs with polycondensation of the sol−gel, resulting in large shrinkage of the film. If the PS particles are burned or melted, the titania gel will reshape into cylinders (in Figure 21b: A1 → A2) to lower the surface tension. After the reshaping, the global shrinkage of the whole structure starts isotropically (A2 → B). However, a local change in the structure cannot always be followed by the whole system. Therefore, the cylinder can only shrink in its radius (B → C), forming a skeleton morphology.

Various sol−gel precursors for SiO_2, ZrO_2, TiO_2, and Al_2O_2 have been studied to form inverse opals.[242,245,258,259] Although fabrication is relatively simple, the sol−gel reaction often lacks the quality and precision of conformal coating by the top-down CVD or ALD process. TiO_2 precursors, e.g. titanium-alkoxides, are typically air/moisture sensitive, making it difficult to control the degree of infiltration in an open environment. In addition, multiple deposition/drying cycles are required to create a robust 3D structure without pattern collapse. However, in any deposition cycle, there is a possibility that the deposition is not confined in the template and/or the residual precursors may block the template, resulting in incomplete filling. There has been a wide range of study to optimize the precursor solution for better infiltration and more uniform coating.[238,244] Recently, Galusha et al. have shown a much improved sol−gel infiltration and processing method, resulting in planar titania inverse opals with controlled thickness and a uniformly flat and open surface without the need of postinfiltration structural etching/milling steps.[238] They prepared the precursor solution by the mixture of titanium−alkoxide and fluorinated organic and strong inorganic acids. Solubilizing titanium-alkoxides together with trifluoroacetic acid molecules form stable building blocks for further cross-linking. In addition, the presence of fluorinated acid improves the hydrophobic character of the precursor, allowing for a more uniform wetting of the polystyrene template. Figure 22 shows the SEM image, band gap diagram, and reflectance spectrum of their TiO_2 inverse

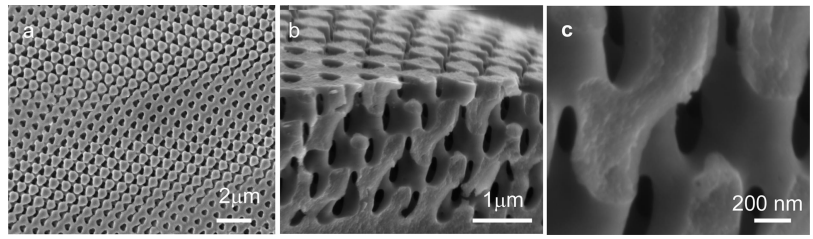

Figure 23. SEM images of 3D inverse titania crystals after preannealing at 375 °C and calcination at 500 °C for 3 h. (a) Top view and (b, c) cross-sectional views at different magnifications. The film was electrodeposited for ~79 min. (Reprinted from ref 239. Copyright 2008 American Chemical Society.)

opals. In addition to the first-order PBG, they can measure the PBG at a higher-frequency region, which is very sensitive to structural defects due to the increased density of optical bands. This reveals the excellent quality of the inverse opals.

3.4. Supercritical Deposition

Supercritical deposition is in between liquid and vapor deposition, where the precursor is deposited onto substrates through supercritical state fluids. Specifically, supercritical carbon dioxide ($scCO_2$) is most frequently used as a medium because of its low cost and formed at low critical temperature and pressure ($T_c = 31$ °C, $P_c = 73.8$ bar).[260] Many ceramic precursors such as metal alkoxides can be dissolved in $scCO_2$.[261] Compared to the liquid phase deposition, $scCO_2$ possesses low viscosity, high diffusivity, and very low surface tension; therefore, the infiltration of precursors can be much improved. Moreover, metal oxide can be selectively deposited on the template surface by controlling the solubility of ceramic precursors in $scCO_2$. Cabanas et al. have showed selective deposition of silica onto a colloidal crystal surface by loading opals, silica precursor (TEOS), and water separately in the high pressure reactor.[262] At the supercritical state, TEOS and water are diffused into $scCO_2$; however, TEOS does not react in the supercritical phase. Instead, the sol−gel reaction occurs only on the particle surface, where the acidic catalyst is absorbed. It should be noted however that many polymer particles can be highly soluble in $scCO_2$.[263,264] For example, the sorption of CO_2 in polystyrene at 40 °C and 85 bar is 12−13 wt %, which reduces the glass transition temperature of polymers. Although the T_g of PS at atmospheric pressure is about 105 °C, it decreases as CO_2 pressure increases, ~ 1 °C/bar up to 60 bar. This limitation can be overcome by addition of cross-linkers during particle synthesis and introduction of polar groups, such as carboxylic acid, on the particle surface. The deposition in $scCO_2$ shows less volume shrinkage after the removal of PS templates and the silica shell coating on inverse opals showed much larger surface areas, in comparison to the case of a conventional liquid phase reaction.

3.5. Electrochemical Deposition

The electrochemical methods have been widely used to deposit metals (e.g., Au, Ag, W, Pt, Pd, Co, Ni, Cu),[256,257] metal chalcogenide (e.g., CdS[221] and CdSe[265]), and semiconductors (e.g., TiO_2[266] and ZnO[267]). Since metals are largely absorbing at visible and near-infrared light itself, previous work has been mainly focused in polymeric and dielectric PCs. Metallic PCs have attracted great attention in recent years due to the potential for new properties and phenomena, including tailored thermal emission,[12] localized surface plasmonic resonance (LSPR),[268,269] as well as PBG properties at IR wavelengths.[270] Gold[268] and silver[271] inverse opals have been formed by electroplating the silica particles, followed by colloidal assembly via sedimentation. Yu et al. have prepared Ni inverse opals and showed the thermal emission properties.[272]

Another unique characteristic of electrochemical deposition is the possibility of complete filling, since the growth starts from the bottom of the structures and then fills the voids toward the surface.[273] Previous experimental studies have shown that it is challenging to completely fill the holographically patterned structures through a top-down evaporation process. Since the pore sizes within the 3D structures are not uniform, the conformally coated pore surface begins to pinch off at the narrowest channels before achieving complete filling. Calculation further confirms that it is nearly impossible to completely fill such templates by a conformal coating process.[251]

Xu et al. recently demonstrated electrodeposition of TiO_2 within an insulating 3D polymer template patterned from HL.[239] The titania precursor solution was prepared by oxidizing titanium powder in acidic solution containing potassium nitrate (KNO_3). The titania electrodeposition occurred in three steps. First, the nitrate ions were electroreduced and generate hydroxide ions, increasing the local pH and hydrolyzing the titania precursor to form a dispersion of sol particles on the charged surface. As the electrochemistry proceeded, the sol particles were cross-linked to form the titanium oxyhydroxide gel network. At the early deposition stage, a thin titania layer appeared to be conformally coated on the SU-8 template. Since the polymer film is an insulator, building up a conformal coating of a TiO_2 thin "seed" layer on the polymer template at the initial stage is a critical step for the subsequent electrodeposition throughout the 3D microporous template. Once the seed layer was established, the deposition proceeded rather quickly. The 3D SU8 template was completely filled in a bottom-up fashion (see Figure 23). In comparison to conventional sol−gel backfilling, electrochemically induced sol−gel reaction offers several advantages that appear attractive for potential complete filling. First, the electrochemistry generates high local pH and a pH gradient within the pore channel, leading to formation of a compact film from the template bottom up[239] and filling small pores (diameter ≤20 nm).[266] Second, the deposition thickness can be controlled by varying the deposition time and current or potential of the counter electrode. Third, the deposition rate could be manipulated by the concentration of electrolyte solution and/or the current or potential of the counter electrode.

3.6. Chemical Reduction

Although inverse high-refractive-index PCs have been demonstrated through various templating approaches (see section 3.1), questions remain as to whether the template is

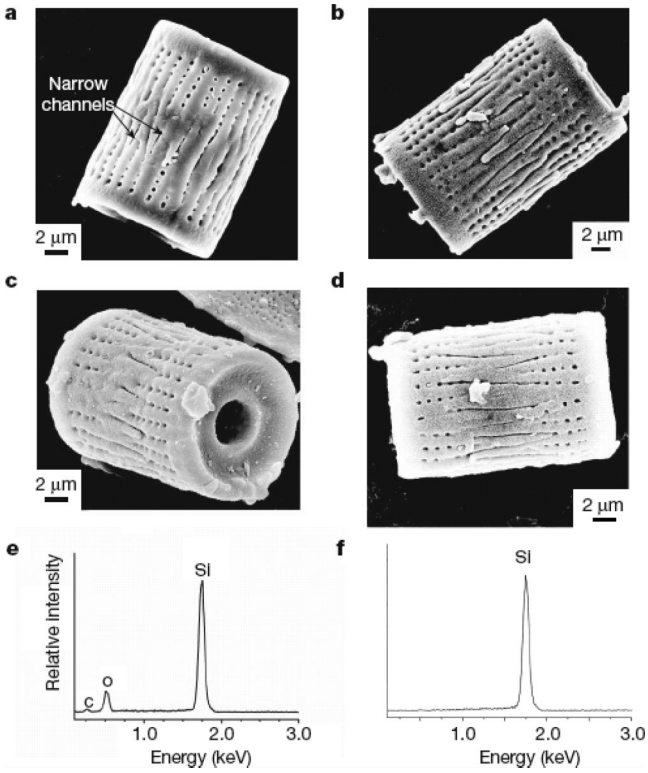

Figure 24. SEM images of (a) Aulacoseira diatom frustules and (b) a MgO/Si composite replica after reaction of an Aulacoseira frustule with Mg(g) at 650 °C for 2.5 h, (c) a silicon-bearing replica produced by selective dissolution of magnesia from a MgO/Si replica in an HCl solution, and (d) a silicon replica after the HCl treatment and an additional treatment in a HF solution. (e, f) Energy dispersive X-ray analyses obtained from silicon frustule replicas of the type shown in parts c and d, respectively. (Reprinted from ref 274. Copyright 2007 Nature Publishing Group.)

completely filled. It is also critical to control the coating thickness, preanneal the backfilled sample, and optimize the heating rate to densify the infiltrated inorganic materials before removal of the polymer template to prevent pattern collapse.[239] Furthermore, the multiple steps involving backfilling and template removal at high temperatures (≥350 °C) could induce defects and cracks. Bao et al.[274] demonstrated a shape-preserving method through magnesiothermic reduction for converting intricate nanostructured silica microshells (frustules) of diatoms (unicellular algae) into microporous nanocrystalline silicon replicas at a relatively low temperature (650 °C) (see Figure 24). The silica nanostructures were converted into cocontinuous, nanocrystalline mixtures of silicon and magnesia by reaction with magnesium gas:

$$2Mg(g) + SiO_2(s) \rightarrow 2MgO(s) + Si(s) \qquad (3)$$

The MgO can be removed by an HCl solution to obtain the Si replica while preserving the original shape. Uniform distribution of silicon and magnesia retains the 3D morphology and nanoscale features (rows of fine pores, narrow channels) during the etching of magnesia. The current yield of reduction is 100 mg h^{-1}; however, it is amenable to scale-up. The shape-preserving magnesiothermic reduction process can be applied to both biological and synthetic silica templates.[275] Therefore, it is possible to engineer the micro- and nanostructures to create large quantities of 3D silicon crystal assemblies with similar or slightly different microscale shapes and nanoscale features for applications, such as chemical and biochemical sensing, and electronic and optical devices.

4. Summary and Outlook

3D PCs that can reflect light from any direction or guide photons potentially offer revolutionary advances in the next-generation microphotonic devices and the integration of existing opto-electronic devices. In the last two decades, there has been a race in developing new techniques to fabricate 3D PC structures with large complete PBGs. In recent years, considerable effort has been directed to explore novel materials that will enable mass production of 3D PCs with controlled size, symmetry, defect(s), and high refractive index over a large area. While self-assembly approaches are simple and the least expensive, they inevitably will introduce random defects during the assembling process. Thus, control of surface chemistry, composition, and concentration of colloidal particles and choice of dispersion medium are critical to the long-range ordering and orientation in colloidal crystals. In comparison, top-down lithography offers an intrinsically defect-free method to create perfect crystalline structures. However, in practice (1) film shrinkage and optical refraction during lithography steps can cause lattice distortion, (2) incomplete filling can decrease the PBG width and optical quality of the film, and (3) low thermal and mechanical stability during backfilling and template removal can lead to pattern collapse and crack formation in the 3D structures. Therefore, investigation and development of high fidelity materials have become pressing issues in 3D fabrication of PCs. However, the materials used in 3D fabrication are rather limited, for example, mostly relying on commercially available SU-8 in interference lithographic processes. In this review, we discuss the recent advances in 3D fabrication of PC structures over a large area from the chemistry point of view. Since the backfilling process is typically required to enhance photonic properties, various backfilling chemistries, e.g. wet vs dry process, double templating vs single templating, and organic vs inorganic templates, are also reviewed. While the dry process, such as CVD and ALD, offers precisely controlled and uniform coatings on a template surface, it requires templates to be thermally and mechanically stable at a high backfilling temperature (typically above 400 °C). In addition, it is very difficult to achieve complete filling by the top-down conformal coating process. In comparison, wet deposition methods offer a broader range of backfilling chemistry and the possibility of complete filling of the porous structures.

It will be ideal if one can combine the benefits of mass-production using self-assembly approaches and of large-scale production using a lithographic process. A few groups have started to couple at least two nonconventional lithographic approaches together in a parallel process and have shown promise for the rapid production of 3D structures with submicrometer periodicity and no defects over a large area (up to cm^2). In addition, there has been rising interest in creating 3D structures from environmentally responsive materials, such as hydrogels, and through infiltration of responsive nanoparticles into the 3D templates. Although these 3D crystals do not possess enough high-refractive-index contrast to obtain complete PBGs, they open a new door to tune the photonic properties (e.g., band gap width and position) and, furthermore, present intriguing new discovery and new phenomena beyond photonic applications, including sensing, microfluidics, tissue scaffold, and mechanical and structural materials.

5. Acknowledgments

S.Y. acknowledges support by the Office of Naval Research (ONR), Grant No. N00014-05-0303, and the Air Force Office of Scientific Research (AFOSR), Grant No. FA9550-06-1-0228. J.H.M. acknowledges support by the Korea Research Foundation Grant funded by the Korean Government (MOEHRD) (KRF-2008-313-D00295), the Manpower Development Program for Energy & Resources of the Ministry of Knowledge and Economy (2008-E-AP-HM-P-23-0000), and Basic Science Research Program through the National Research Foundation of Korea (NRF) funded by the Ministry of Education, Science and Technology (2009-0069998).

6. References

(1) Joannopoulos, J. D.; Meade, R. D.; Winn, J. N. *Photonic Crystals*; Princeton University Press: Princeton, NJ, 1995.
(2) Lin, S. Y.; Fleming, J. G.; Hetherington, D. L.; Smith, B. K.; Biswas, R.; Ho, K. M.; Sigalas, M. M.; Zubrzycki, W.; Kurtz, S. R.; Bur, J. *Nature* **1998**, *394*, 251.
(3) Johnson, S. G.; Joannopoulos, J. D. *Appl. Phys. Lett.* **2000**, *77*, 3490.
(4) Aoki, K.; Miyazaki, H. T.; Hirayama, H.; Inoshita, K.; Baba, T.; Sakoda, K.; Shinya, N.; Aoyagi, Y. *Nat. Mater.* **2003**, *2*, 117.
(5) Ozin, G. A.; Yang, S. M. *Adv. Funct. Mater.* **2001**, *11*, 95.
(6) Edrington, A. C.; Urbas, A. M.; DeRege, P.; Chen, C. X.; Swager, T. M.; Hadjichristidis, N.; Xenidou, M.; Fetters, L. J.; Joannopoulos, J. D.; Fink, Y.; Thomas, E. L. *Adv. Mater.* **2001**, *13*, 421.
(7) Zein, I.; Hutmacher, D. W.; Tan, K. C.; Teoh, S. H. *Biomaterials* **2002**, *23*, 1169.
(8) Vozzi, G.; Flaim, C.; Ahluwaliaa, A.; Bhatia, S. *Biomaterials* **2003**, *24*, 2533.
(9) Chelnokov, A.; Wang, K.; Rowson, S.; Garoche, P.; Lourtioz, J. M. *Appl. Phys. Lett.* **2000**, *77*, 2943.
(10) Gratson, G. M.; Garcia-Santamaria, F.; Lousse, V.; Xu, M. J.; Fan, S. H.; Lewis, J. A.; Braun, P. V. *Adv. Mater.* **2006**, *18*, 461.
(11) Lee, J. H.; Kim, C. H.; Ho, K. M.; Constant, K. *Adv. Mater.* **2005**, *17*, 2481.
(12) Lee, J. H.; Kim, Y. S.; Constant, K.; Ho, K. M. *Adv. Mater.* **2007**, *19*, 791.
(13) Lee, J. H.; Leung, W.; Ahn, J.; Lee, T.; Park, I. S.; Constant, K.; Ho, K. M. *Appl. Phys. Lett.* **2007**, *90*.
(14) Kennedy, S. R.; Brett, M. J.; Toader, O.; John, S. *Nano Lett.* **2002**, *2*, 59.
(15) Summers, M. A.; Brett, M. J. *Nanotechnology* **2008**, *19*, 415203.
(16) Campbell, M.; Sharp, D. N.; Harrison, M. T.; Denning, R. G.; Turberfield, A. J. *Nature* **2000**, *404*, 53.
(17) Yang, S.; Megens, M.; Aizenberg, J.; Wiltzius, P.; Chaikin, P. M.; Russel, W. B. *Chem. Mater.* **2002**, *14*, 2831.
(18) Miklyaev, Y. V.; Meisel, D. C.; Blanco, A.; von Freymann, G.; Busch, K.; Koch, W.; Enkrich, C.; Deubel, M.; Wegener, M. *Appl. Phys. Lett.* **2003**, *82*, 1284.
(19) Ullal, C. K.; Maldovan, M.; Wohlgemuth, M.; Thomas, E. L. *J. Opt. Soc. Am. A* **2003**, *20*, 948.
(20) Ullal, C. K.; Maldovan, M.; Thomas, E. L.; Chen, G.; Han, Y.-J.; Yang, S. *Appl. Phys. Lett.* **2004**, *84*, 5434.
(21) Meisel, D. C.; Diem, M.; Deubel, M.; Perez-Willard, F.; Linden, S.; Gerthsen, D.; Busch, K.; Wegener, M. *Adv. Mater.* **2006**, *18*, 2964.
(22) Moon, J. H.; Ford, J.; Yang, S. *Polym. Adv. Technol.* **2006**, *17*, 83.
(23) Jang, J. H.; Ullal, C. K.; Maldovan, M.; Gorishnyy, T.; Kooi, S.; Koh, C. Y.; Thomas, E. L. *Adv. Funct. Mater.* **2007**, *17*, 3027.
(24) Jeon, S.; Park, J. U.; Cirelli, R.; Yang, S.; Heitzman, C. E.; Braun, P. V.; Kenis, P. J. A.; Rogers, J. A. *Proc. Natl. Acad. Sci. U.S.A.* **2004**, *101*, 12428.
(25) Jeon, S.; Menard, E.; Park, J. U.; Maria, J.; Meitl, M.; Zaumseil, J.; Rogers, J. A. *Adv. Mater.* **2004**, *16*, 1369.
(26) Jeon, S.; Nam, Y. S.; Shir, D. J. L.; Rogers, J. A.; Hamza, A. *Appl. Phys. Lett.* **2006**, *89*.
(27) Shir, D. J.; Jeon, S.; Liao, H.; Highland, M.; Cahill, D. G.; Su, M. F.; El-Kady, I. F.; Christodoulou, C. G.; Bogart, G. R.; Hamza, A. V.; Rogers, J. A. *J. Phys. Chem. B* **2007**, *111*, 12945.
(28) Shir, D.; Liao, H. W.; Jeon, S.; Xiao, D.; Johnson, H. T.; Bogart, G. R.; Bogart, K. H. A.; Rogers, J. A. *Nano Lett.* **2008**, *8*, 2236.
(29) Lin, Y.; Herman, P. R.; Darmawikarta, K. *Appl. Phys. Lett.* **2005**, *86*, 071117.
(30) Chan, T. Y. M.; Toader, O.; John, S. *Phys. Rev. E* **2006**, *73*.
(31) Lin, Y. K.; Harb, A.; Rodriguez, D.; Lozano, K.; Xu, D.; Chen, K. P. *Opt. Express* **2008**, *16*, 9165.
(32) Rinne, J. W.; Gupta, S.; Wiltzius, P. *Opt. Express* **2008**, *16*, 663.
(33) Cumpston, B. H.; Ananthavel, S. P.; Barlow, S.; Dyer, D. L.; Ehrlich, J. E.; Erskine, L. L.; Heikal, A. A.; Kuebler, S. M.; Lee, I. Y. S.; McCord-Maughon, D.; Qin, J. Q.; Rockel, H.; Rumi, M.; Wu, X. L.; Marder, S. R.; Perry, J. W. *Nature* **1999**, *398*, 51.
(34) Kawata, S.; Sun, H. B.; Tanaka, T.; Takada, K. *Nature* **2001**, *412*, 697.
(35) Bratton, D.; Yang, D.; Dai, J. Y.; Ober, C. K. *Polym. Adv. Technol.* **2006**, *17*, 94.
(36) Lee, K. S.; Yang, D. Y.; Park, S. H.; Kim, R. H. *Polym. Adv. Technol.* **2006**, *17*, 72.
(37) Marder, S. R.; Bredas, J. L.; Perry, J. W. *MRS Bull.* **2007**, *32*, 561.
(38) Ho, K. M.; Chan, C. T.; Soukoulis, C. M. *Phys. Rev. Lett.* **1990**, *65*, 3152.
(39) Maldovan, M.; Urbas, A. M.; Yufa, N.; Carter, W. C.; Thomas, E. L. *Phys. Rev. B* **2002**, *65*, 165123.
(40) Maldovan, M.; Thomas, E. L. *Nat. Mater.* **2004**, *3*, 593.
(41) Ren, Z.; Wang, Z.; Zhai, T.; Gao, H.; Liu, D.; Zhang, X. D. *Phys. Rev. B* **2007**, *76*.
(42) Arsenault, A. C.; Puzzo, D. P.; Ghoussoub, A.; Manners, I.; Ozin, G. A. *J. Soc. Inf. Disp.* **2007**, *15*, 1095.
(43) Ha, N. Y.; Ohtsuka, Y.; Jeong, S. M.; Nishimura, S.; Suzaki, G.; Takanishi, Y.; Ishikawa, K.; Takezoe, H. *Nat. Mater.* **2008**, *7*, 43.
(44) Holtz, J. H.; Asher, S. A. *Nature* **1997**, *389*, 829.
(45) Holtz, J. H.; Holtz, J. S. W.; Munro, C. H.; Asher, S. A. *Anal. Chem.* **1998**, *70*, 780.
(46) Lee, K.; Asher, S. A. *J. Am. Chem. Soc.* **2000**, *122*, 9534.
(47) Li, H. L.; Wang, J. X.; Yang, L. M.; Song, Y. L. *Adv. Funct. Mater.* **2008**, *18*, 3258.
(48) Li, M. Z.; He, F.; Liao, Q.; Liu, J.; Xu, L.; Jiang, L.; Song, Y. L.; Wang, S.; Zhu, D. B. *Angew. Chem., Int. Ed.* **2008**, *47*, 7258.
(49) Xu, M.; Goponenko, A. V.; Asher, S. A. *J. Am. Chem. Soc.* **2008**, *130*, 3113.
(50) Noda, S.; Fujita, M.; Asano, T. *Nat. Photonics* **2007**, *1*, 449.
(51) Galli, M.; Portalupi, S. L.; Belotti, M.; Andreani, L. C.; O'Faolain, L.; Krauss, T. F. *Appl. Phys. Lett.* **2009**, *94*, 3.
(52) Mao, H. B.; Jing, W. P. *J. Microlithogr., Microfabr., Microsyst.* **2005**, *4*, 041301.
(53) Mao, D.; Ouyang, Z.; Wang, J. C.; Liu, C. P.; Wu, C. J. *Appl. Phys. B: Lasers Opt.* **2008**, *90*, 127.
(54) Noda, S.; Yokoyama, M.; Imada, M.; Chutinan, A.; Mochizuki, M. *Science* **2001**, *293*, 1123.
(55) Solli, D. R.; McCormick, C. F.; Chiao, R. Y.; Hickmann, J. M. *J. Appl. Phys.* **2003**, *93*, 9429.
(56) Thiel, M.; Hermatschweiler, M.; Wegener, M.; von Freymann, G. *Appl. Phys. Lett.* **2007**, *91*, 3.
(57) Xu, X. L.; Friedman, G.; Humfeld, K. D.; Majetich, S. A.; Asher, S. A. *Adv. Mater.* **2001**, *13*, 1681.
(58) Xu, X. L.; Majetich, S. A.; Asher, S. A. *J. Am. Chem. Soc.* **2002**, *124*, 13864.
(59) Saado, Y.; Golosovsky, M.; Davidov, D.; Frenkel, A. *Phys. Rev. B* **2002**, *66*, 195108.
(60) Camargo, P. H. C.; Li, Z. Y.; Xia, Y. *Soft Matter* **2007**, *3*, 1215.
(61) Ge, J. P.; Hu, Y. X.; Yin, Y. D. *Angew. Chem., Int. Ed.* **2007**, *46*, 7428.
(62) Mach, P.; Wiltzius, P.; Megens, M.; Weitz, D. A.; Lin, K. H.; Lubensky, T. C.; Yodh, A. G. *Phy. Rev. E* **2002**, *65*, 031720.
(63) Gaillot, D. P.; Graugnard, E.; King, J. S.; Summers, C. J. *J. Opt. Soc. Am. B* **2007**, *24*, 990.
(64) Lee, Y. J.; Braun, P. V. *Adv. Mater.* **2003**, *15*, 563.
(65) Barry, R. A.; Wiltzius, P. *Langmuir* **2006**, *22*, 1369.
(66) Liu, Y. F.; Wang, S. P. *Colloids Surf., B* **2007**, *58*, 8.
(67) Wang, J. Y.; Cao, Y.; Feng, Y.; Yin, F.; Gao, J. P. *Adv. Mater.* **2007**, *19*, 3865.
(68) Kang, J. H.; Moon, J. H.; Lee, S. K.; Park, S. G.; Jang, S. G.; Yang, S.; Yang, S. M. *Adv. Mater.* **2008**, *20*, 3061.
(69) Jang, J. H.; Jhaveri, S. J.; Rasin, B.; Koh, C.; Ober, C. K.; Thomas, E. L. *Nano Lett.* **2008**, *8*, 1456.
(70) Yoon, J.; Lee, W.; Thomas, E. L. *MRS Bull.* **2005**, *30*, 721.
(71) Xia, Y. N.; Gates, B.; Li, Z. Y. *Adv. Mater.* **2001**, *13*, 409.
(72) Bates, F. S.; Fredrickson, G. H. *Annu. Rev. Phys. Chem.* **1990**, *41*, 525.
(73) Zheng, W.; Wang, Z.-G. *Macromolecules* **1995**, *28*, 7215.
(74) Black, C. T.; Guarini, K. W.; Milkove, K. R.; Baker, S. M.; Russell, T. P.; Tuominen, M. T. *Appl. Phys. Lett.* **2001**, *79*, 409.
(75) Kim, S. O.; Solak, H. H.; Stoykovich, M. P.; Ferrier, N. J.; de Pablo, J. J.; Nealey, P. F. *Nature* **2003**, *424*, 411.
(76) Kim, S. H.; Misner, M. J.; Xu, T.; Kimura, M.; Russell, T. P. *Adv. Mater.* **2004**, *16*, 226.
(77) Stoykovich, M. P.; Muller, M.; Kim, S. O.; Solak, H. H.; Edwards, E. W.; de Pablo, J. J.; Nealey, P. F. *Science* **2005**, *308*, 1442.
(78) So, Y. H.; Hahn, S. F.; Li, Y. F.; Reinhard, M. T. *J. Polym. Sci., Part A: Polym. Chem.* **2008**, *46*, 2799.

(79) Jung, Y. S.; Jung, W.; Tuller, H. L.; Ross, C. A. *Nano Lett.* **2008**, *8*, 3776.
(80) Fink, Y.; Urbas, A. M.; Bawendi, M. G.; Joannopoulos, J. D.; Thomas, E. L. *J. Lightwave Technol.* **1999**, *17*, 1963.
(81) Urbas, A.; Sharp, R.; Fink, Y.; Thomas, E. L.; Xenidou, M.; Fetters, L. J. *Adv. Mater.* **2000**, *12*, 812.
(82) Urbas, A. M.; Maldovan, M.; DeRege, P.; Thomas, E. L. *Adv. Mater.* **2002**, *14*, 1850.
(83) Maldovan, M.; Ullal, C. K.; Jang, J. H.; Thomas, E. L. *Adv. Mater.* **2007**, *19*, 3809.
(84) Kim, S. H.; Misner, M. J.; Russell, T. P. *Adv. Mater.* **2004**, *16*, 2119.
(85) Stoykovich, M. P.; Kang, H.; Daoulas, K. C.; Liu, G.; Liu, C. C.; de Pablo, J. J.; Mueller, M.; Nealey, P. F. *ACS Nano* **2007**, *1*, 168.
(86) Bita, I.; Yang, J. K. W.; Jung, Y. S.; Ross, C. A.; Thomas, E. L.; Berggren, K. K. *Science* **2008**, *321*, 939.
(87) Park, C.; De Rosa, C.; Fetters, L. J.; Lotz, B.; Thomas, E. L. *Adv. Mater.* **2001**, *13*, 724.
(88) Tsori, Y.; Tournilhac, F.; Leibler, L. *Macromolecules* **2003**, *36*, 5873.
(89) Olszowka, V.; Hund, M.; Kuntermann, V.; Scherdel, S.; Tsarkova, L.; Boker, A.; Krausch, G. *Soft Matter* **2006**, *2*, 1089.
(90) Pinna, M.; Zvelindovsky, A. V. *Soft Matter* **2008**, *4*, 316.
(91) Osuji, C.; Ferreira, P. J.; Mao, G. P.; Ober, C. K.; Vander Sande, J. B.; Thomas, E. L. *Macromolecules* **2004**, *37*, 9903.
(92) Angelescu, D. E.; Waller, J. H.; Adamson, D. H.; Deshpande, P.; Chou, S. Y.; Register, R. A.; Chaikin, P. M. *Adv. Mater.* **2004**, *16*, 1736.
(93) Angelescu, D. E.; Waller, J. H.; Adamson, D. H.; Register, R. A.; Chaikin, P. M. *Adv. Mater.* **2007**, *19*, 2687.
(94) Voicu, N. E.; Ludwigs, S.; Steiner, U. *Adv. Mater.* **2008**, *20*, 3022.
(95) Harrison, C.; Cheng, Z. D.; Sethuraman, S.; Huse, D. A.; Chaikin, P. M.; Vega, D. A.; Sebastian, J. M.; Register, R. A.; Adamson, D. H. *Phys. Rev. E* **2002**, *66*, 011706.
(96) Fukunaga, K.; Elbs, H.; Magerle, R.; Krausch, G. *Macromolecules* **2000**, *33*, 947.
(97) Osuji, C.; Chao, C. Y.; Bita, I.; Ober, C. K.; Thomas, E. L. *Adv. Funct. Mater.* **2002**, *12*, 753.
(98) Bockstaller, M. R.; Thomas, E. L. *J. Phys. Chem. B* **2003**, *107*, 10017.
(99) Valkama, S.; Kosonen, H.; Ruokolainen, J.; Haatainen, T.; Torkkeli, M.; Serimaa, R.; Ten Brinke, G.; Ikkala, O. *Nat. Mater.* **2004**, *3*, 872.
(100) Kang, Y.; Walish, J. J.; Gorishnyy, T.; Thomas, E. L. *Nat. Mater.* **2007**, *6*, 957.
(101) Fudouzi, H.; Xia, Y. N. *Langmuir* **2003**, *19*, 9653.
(102) Arsenault, A. C.; Clark, T. J.; Von Freymann, G.; Cademartiri, L.; Sapienza, R.; Bertolotti, J.; Vekris, E.; Wong, S.; Kitaev, V.; Manners, I.; Wang, R. Z.; John, S.; Wiersma, D.; Ozin, G. A. *Nat. Mater.* **2006**, *5*, 179.
(103) Giddings, J. C. *Science* **1993**, *260*, 1456.
(104) van Blaaderen, A.; Ruel, R.; Wiltzius, P. *Nature* **1997**, *385*, 321.
(105) Holgado, M.; Garcia-Santamaria, F.; Blanco, A.; Ibisate, M.; Cintas, A.; Miguez, H.; Serna, C. J.; Molpeceres, C.; Requena, J.; Mifsud, A.; Meseguer, F.; Lopez, C. *Langmuir* **1999**, *15*, 4701.
(106) Vaudreuil, S.; Bousmina, M.; Kaliaguine, S.; Bonneviot, L. *Adv. Mater.* **2001**, *13*, 1310.
(107) Hoogenboom, J. P.; Derks, D.; Vergeer, P.; van Blaaderen, A. *J. Chem. Phys.* **2002**, *117*, 11320.
(108) Zhou, S. Q.; Sun, H. W. *J. Phys.Chem. B* **2005**, *109*, 6397.
(109) Dolbnya, I. P.; Petukhov, A. V.; Aarts, D.; Vroege, G. J.; Lekkerkerker, H. N. W. *Europhys. Lett.* **2005**, *72*, 962.
(110) Norris, D. J.; Arlinghaus, E. G.; Meng, L. L.; Heiny, R.; Scriven, L. E. *Adv. Mater.* **2004**, *16*, 1393.
(111) Brewer, D. D.; Allen, J.; Miller, M. R.; de Santos, J. M.; Kumar, S.; Norris, D. J.; Tsapatsis, M.; Scriven, L. E. *Langmuir* **2008**, *24*, 13683.
(112) Reese, C. E.; Guerrero, C. D.; Weissman, J. M.; Lee, K.; Asher, S. A. *J. Colloid Interface Sci.* **2000**, *232*, 76.
(113) Allard, M.; Sargent, E. H. *Appl. Phys. Lett.* **2004**, *85*, 5887.
(114) Deng, T. S.; Zhang, Q. F.; Zhang, J. Y.; Shen, X.; Zhu, K. T.; Wu, J. L. *J. Colloid Interface Sci.* **2009**, *329*, 292.
(115) Lange, B.; Fleischhaker, F.; Zentel, R. *Macromol. Rapid Commun.* **2007**, *28*, 1291.
(116) Lange, B.; Zentel, R.; Ober, C.; Marder, S. *Chem. Mater.* **2004**, *16*, 5286.
(117) Moon, J. H.; Kim, W. S.; Ha, J.-W.; Jang, S. G.; Yang, S.-M.; Park, J.-K. *Chem. Commun.* **2005**, 4107.
(118) Stöber, W.; Fink, A.; Bohn, E. *J. Colloid Interface Sci.* **1968**, *26*, 62.
(119) Jeong, U.; Wang, Y. L.; Ibisate, M.; Xia, Y. N. *Adv. Funct. Mater.* **2005**, *15*, 1907.
(120) Jiang, X. C.; Herricks, T.; Xia, Y. N. *Adv. Mater.* **2003**, *15*, 1205.
(121) Denkov, N. D.; Velev, O. D.; Kralchevsky, P. A.; Ivanov, I. B.; Yoshimura, H.; Nagayama, K. *Nature* **1993**, *361*, 26.
(122) Jiang, P.; Bertone, J. F.; Hwang, K. S.; Colvin, V. L. *Chem. Mater.* **1999**, *11*, 2132.
(123) Braun, P. V.; Zehner, R. W.; White, C. A.; Weldon, M. K.; Kloc, C.; Patel, S. S.; Wiltzius, P. *Adv. Mater.* **2001**, *13*, 721.
(124) Prevo, B. G.; Kuncicky, D. M.; Velev, O. D. *Colloid Surf., A* **2007**, *311*, 2.
(125) Ko, Y. G.; Shin, D. H. *J. Phys. Chem. B* **2007**, *111*, 1545.
(126) Gasperino, D.; Meng, L. L.; Norris, D. J.; Derby, J. J. *J. Cryst. Growth* **2008**, *310*, 131.
(127) Zheng, Z. Y.; Gao, K. Y.; Luo, Y. H.; Li, D. M.; Meng, Q. B.; Wang, Y. R.; Zhangt, D. Z. *J. Am. Chem. Soc.* **2008**, *130*, 9785.
(128) Kanai, T.; Sawada, T.; Toyotama, A.; Kitamura, K. *Adv. Funct. Mater.* **2005**, *15*, 25.
(129) Jiang, P.; McFarland, M. J. *J. Am. Chem. Soc.* **2004**, *126*, 13778.
(130) Jiang, P. *Chem. Commun.* **2005**, 1699.
(131) Min, W. L.; Jiang, P.; Jiang, B. *Nanotechnology* **2008**, *19*, 475604.
(132) Mihi, A.; Ocaña, M.; Míguez, H. *Adv. Mater.* **2006**, *18*, 2244.
(133) Wang, L. K.; Zhao, X. S. *J. Phys. Chem. C* **2007**, *111*, 8538.
(134) Piret, F.; Su, B. L. *Chem. Phys. Lett.* **2008**, *457*, 376.
(135) Yamanaka, J.; Murai, M.; Iwayama, Y.; Yonese, M. S.; Ito, K.; Sawada, T. *J. Am. Chem. Soc.* **2004**, *126*, 7156.
(136) Wakabayashi, N.; Yamanaka, J.; Murai, M.; Ito, K.; Sawada, T.; Yonese, M. *Langmuir* **2006**, *22*, 7936.
(137) Murai, M.; Yamada, H.; Yamanaka, J.; Onda, S.; Yonese, M.; Ito, K.; Sawada, T.; Uchida, F.; Ohki, Y. *Langmuir* **2007**, *23*, 7510.
(138) Bevan, M. A.; Lewis, J. A.; Braun, P. V.; Wiltzius, P. *Langmuir* **2004**, *20*, 7045.
(139) Rodner, S. C.; Wedin, P.; Bergstrom, L. *Langmuir* **2002**, *18*, 9327.
(140) Alexeev, V. L.; Sharma, A. C.; Goponenko, A. V.; Das, S.; Lednev, I. K.; Wilcox, C. S.; Finegold, D. N.; Asher, S. A. *Anal. Chem.* **2003**, *75*, 2316.
(141) Lee, Y. J.; Pruzinsky, S. A.; Braun, P. V. *Langmuir* **2004**, *20*, 3096.
(142) Huang, J.; Hu, X. B.; Zhang, W. X.; Zhang, Y. H.; Li, G. T. *Colloid Polym. Sci.* **2008**, *286*, 113.
(143) Wijnhoven, J.; Vos, W. L. *Science* **1998**, *281*, 802.
(144) Juárez, B. H.; Ibisate, M.; Palacios, J. M.; López, C. *Adv. Mater.* **2003**, *15*, 319.
(145) Ngo, T. T.; Liddell, C. M.; Ghebrebrhan, M.; Joannopoulos, J. D. *Appl. Phys. Lett.* **2006**, *88*, 241920.
(146) Hynninen, A. P.; Thijssen, J. H. J.; Vermolen, E. C. M.; Dijkstra, M.; Van Blaaderen, A. *Nat. Mater.* **2007**, *6*, 202.
(147) Shevchenko, E. V.; Talapin, D. V.; Kotov, N. A.; O'Brien, S.; Murray, C. B. *Nature* **2006**, *439*, 55.
(148) Leunissen, M. E.; Christova, C. G.; Hynninen, A. P.; Royall, C. P.; Campbell, A. I.; Imhof, A.; Dijkstra, M.; van Roij, R.; van Blaaderen, A. *Nature* **2005**, *437*, 235.
(149) Bita, I.; Choi, T.; Walsh, M. E.; Smith, H. L.; Thomas, E. L. *Adv. Mater.* **2007**, *19*, 1403.
(150) Petsas, K. I.; Coates, A. B.; Grynberg, G. *Phys. Rev. A* **1994**, *50*, 5173.
(151) Thompson, L. F.; Willson, C. G.; Bowden, M. J. *Introduction to Microlithography*, 2nd ed.; American Chemical Society: Washington, DC, 1994.
(152) Wu, L. J.; Zhong, Y. C.; Chan, C. T.; Wong, K. S.; Wang, G. P. *Appl. Phys. Lett.* **2005**, *86*, 3.
(153) Yang, S.; Chen, G.; Megens, M.; Ullal, C. K.; Han, Y. J.; Rapaport, R.; Thomas, E. L.; Aizenberg, J. *Adv. Mater.* **2005**, *17*, 435.
(154) Moon, J. H.; Yang, S.; Dong, W. T.; Perry, J. W.; Adibi, A.; Yang, S. M. *Opt. Express* **2006**, *14*, 6297.
(155) Wang, X.; Ng, C. Y.; Tam, W. Y.; Chan, C. T.; Sheng, P. *Adv. Mater.* **2003**, *15*, 1526.
(156) Yang, Y.; Zhang, S. H.; Wang, G. P. *Appl. Phys. Lett.* **2006**, *88*, 51104.
(157) Mao, W. D.; Dong, J. W.; Zhong, Y. C.; Liang, G. Q.; Wang, H. Z. *Opt. Express* **2005**, *13*, 2994.
(158) Mao, W. D.; Liang, G. Q.; Pu, Y. Y.; Wang, H. Z.; Zeng, Z. H. *Appl. Phys. Lett.* **2007**, *91*, 3.
(159) Lin, Y. K.; Rivera, D.; Chen, K. P. *Opt. Express* **2006**, *14*, 887.
(160) Shaw, J. M.; Gelorme, J. D.; LaBianca, N. C.; Conley, W. E.; Holmes, S. J. *IBM J. Res. Dev.* **1997**, *41*, 81.
(161) Lee, K. Y.; LaBianca, N.; Rishton, S. A.; Zolgharnain, S.; Gelorme, J. D.; Shaw, J.; Chang, T. H. P. *J. Vac. Sci. Technol., B* **1995**, *13*, 3012.
(162) Lorenz, H.; Despont, M.; Vettiger, P.; Renaud, P. *Microsyst. Technol.* **1998**, *4*, 143.
(163) Lorenz, H.; Despont, M.; Fahrni, N.; LaBianca, N.; Renaud, P.; Vettiger, P. *J. Micromech. Microeng.* **1997**, *7*, 121.
(164) Ribeiro, J. C.; Minas, G.; Turmezei, P.; Wolffenbuttel, R. F.; Correia, J. H. *Sens. Actuator A* **2005**, *123−24*, 77.
(165) Lorenz, H.; Despont, M.; Fahrni, N.; Brugger, J.; Vettiger, P.; Renaud, P. *Sens. Actuator A* **1998**, *64*, 33.
(166) Bertsch, A.; Lorenz, H.; Renaud, P. *Sens. Actuator A* **1999**, *73*, 14.
(167) Bogdanov, A. L.; Peredkov, S. S. *Microelectron. Eng.* **2000**, *53*, 493.
(168) Wang, Y. L.; Pai, J. H.; Lai, H. H.; Sims, C. E.; Bachman, M.; Li, G. P.; Allbritton, N. L. *J. Micromech. Microeng.* **2007**, *17*, 1371.

(169) Kastantin, M. J.; Li, S.; Gadre, A. P.; Wu, L. Q.; Bentley, W. E.; Payne, G. F.; Rubloff, G. W.; Ghodssi, R. *Sens. Mater.* **2003**, *15*, 295.
(170) Crivello, J. V.; Lam, J. H. W. *J. Polym. Sci.: Polym. Chem. Ed.* **1978**, *16*, 2441.
(171) Bi, Y. B.; Neckers, D. C. *Macromolecules* **1994**, *27*, 3683.
(172) Hua, Y. J.; Crivello, J. V. *Macromolecules* **2001**, *34*, 2488.
(173) Moon, J. H.; Yang, S. M.; Pine, D. J.; Chang, W. S. *Appl. Phys. Lett.* **2004**, *85*, 4184.
(174) Moon, J. H.; Small, A.; Yi, G. R.; Lee, S. K.; Chang, W. S.; Pine, D. J.; Yang, S. M. *Synth. Met.* **2005**, *148*, 99.
(175) Wang, X.; Xu, J. F.; Su, H. M.; Zeng, Z. H.; Chen, Y. L.; Wang, H. Z.; Pang, Y. K.; Tam, W. Y. *Appl. Phys. Lett.* **2003**, *82*, 2212.
(176) Zhu, X. L.; Xu, Y. G.; Yang, S. *Opt. Express* **2007**, *15*, 16546.
(177) Kondo, T.; Juodkazis, S.; Misawa, H. *Appl. Phys. A: Mater. Sci. Process.* **2005**, *81*, 1583.
(178) Hayek, A.; Xu, Y. G.; Okada, T.; Barlow, S.; Zhu, X. L.; Moon, J. H.; Marder, S. R.; Yang, S. *J. Mater. Chem.* **2008**, *18*, 3316.
(179) Zhou, W. H.; Kuebler, S. M.; Braun, K. L.; Yu, T. Y.; Cammack, J. K.; Ober, C. K.; Perry, J. W.; Marder, S. R. *Science* **2002**, *296*, 1106.
(180) Yu, T. Y.; Ober, C. K.; Kuebler, S. M.; Zhou, W. H.; Marder, S. R.; Perry, J. W. *Adv. Mater.* **2003**, *15*, 517.
(181) Jang, J. H.; Ullal, C. K.; Gorishnyy, T.; Tsukruk, V. V.; Thomas, E. L. *Nano Lett.* **2006**, *6*, 740.
(182) Saravanamuttu, K.; Blanford, C. F.; Sharp, D. N.; Dedman, E. R.; Turberfield, A. J.; Denning, R. G. *Chem. Mater.* **2003**, *15*, 2301.
(183) Salauen, M.; Audier, M.; Delyon, F.; Duneau, M. *Appl. Surf. Sci.* **2007**, *254*, 830.
(184) Shishido, A.; Diviliansky, I. B.; Khoo, I. C.; Mayer, T. S.; Nishimura, S.; Egan, G. L.; Mallouk, T. E. *Appl. Phys. Lett.* **2001**, *79*, 3332.
(185) Cho, J. D.; Ju, H. T.; Park, Y. S.; Hong, J. W. *Macromol. Mater. Eng.* **2006**, *291*, 1155.
(186) Moon, J. H.; Seo, J. S.; Xu, Y.; Yang, S. *J. Mater. Chem.* **2009**, *19*, 4687.
(187) Matějeka, L.; Strachota, A.; Pleštil, J.; Whelan, P.; Steinhart, M.; Šlouf, M. *Macromolecules* **2004**, *37*, 9449.
(188) Luo, Q. Z.; Mutlu, S.; Gianchandani, Y. B.; Svec, F.; Frechet, J. M. J. *Electrophoresis* **2003**, *24*, 3694.
(189) Zhang, Y. J.; Wang, S. P.; Eghtedari, M.; Motamedi, M.; Kotov, N. A. *Adv. Funct. Mater.* **2005**, *15*, 725.
(190) Yang, S.; Ford, J.; Ruengruglikit, C.; Huang, Q. R.; Aizenberg, J. *J. Mater. Chem.* **2005**, *15*, 4200.
(191) Haske, W.; Chen, V. W.; Hales, J. M.; Dong, W. T.; Barlow, S.; Marder, S. R.; Perry, J. W. *Opt. Express* **2007**, *15*, 3426.
(192) Sun, H. B.; Matsuo, S.; Misawa, H. *Appl. Phys. Lett.* **1999**, *74*, 786.
(193) Sun, H. B.; Tanaka, T.; Takada, K.; Kawata, S. *Appl. Phys. Lett.* **2001**, *79*, 1411.
(194) Chowdhury, Z. R.; Fedosejevs, R. *Microsyst. Technol.* **2008**, *14*, 59.
(195) Jeon, S.; Malyarchuk, V.; Rogers, J. A.; Wiederrecht, G. P. *Opt. Express* **2006**, *14*, 2300.
(196) Rumi, M.; Ehrlich, J. E.; Heikal, A. A.; Perry, J. W.; Barlow, S.; Hu, Z. Y.; McCord-Maughon, D.; Parker, T. C.; Rockel, H.; Thayumanavan, S.; Marder, S. R.; Beljonne, D.; Bredas, J. L. *J. Am. Chem. Soc.* **2000**, *122*, 9500.
(197) Belfield, K. D.; Ren, X. B.; Van Stryland, E. W.; Hagan, D. J.; Dubikovsky, V.; Miesak, E. J. *J. Am. Chem. Soc.* **2000**, *122*, 1217.
(198) Belfield, K. D.; Schafer, K. J.; Liu, Y. U.; Liu, J.; Ren, X. B.; Van Stryland, E. W. *J. Phys. Org. Chem.* **2000**, *13*, 837.
(199) Belfield, K. D.; Schafer, K. J.; Mourad, W.; Reinhardt, B. A. *J. Org. Chem.* **2000**, *65*, 4475.
(200) Infuehr, R.; Pucher, N.; Heller, C.; Lichtenegger, H.; Liska, R.; Schmidt, V.; Kuna, L.; Haase, A.; Stampfl, J. *Appl. Surf. Sci.* **2007**, *254*, 836.
(201) Lee, W. M.; Pruzinsky, S. A.; Braun, P. V. *Adv. Mater.* **2002**, *14*, 271.
(202) Deubel, M.; Wegener, M.; Kaso, A.; John, S. *Appl. Phys. Lett.* **2004**, *85*, 1895.
(203) Deubel, M.; Von Freymann, G.; Wegener, M.; Pereira, S.; Busch, K.; Soukoulis, C. M. *Nat. Mater.* **2004**, *3*, 444.
(204) Steidl, L.; Jhaveri, S. J.; Ayothi, R.; Sha, J.; McMullen, J. D.; Ng, S. Y. C.; Zipfel, W. R.; Zentel, R.; Ober, C. K. *J. Mater. Chem.* **2009**, *19*, 505.
(205) Coenjarts, C. A.; Ober, C. K. *Chem. Mater.* **2004**, *16*, 5556.
(206) Houbertz, R. *Appl. Surf. Sci.* **2005**, *247*, 504.
(207) Jun, Y.; Nagpal, P.; Norris, D. J. *Adv. Mater.* **2008**, *20*, 606.
(208) George, M. C.; Nelson, E. C.; Rogers, J. A.; Braun, P. V. *Angew. Chem., Int. Ed.* **2009**, *48*, 144.
(209) Ovsianikov, A.; Viertl, J.; Chichkov, B.; Oubaha, M.; MacCraith, B.; Sakellari, L.; Giakoumaki, A.; Gray, D.; Vamvakaki, M.; Farsari, M.; Fotakis, C. *ACS Nano* **2008**, *2*, 2257.
(210) Ovsianikov, A.; Shizhou, X.; Farsari, M.; Vamvakaki, M.; Fotakis, C.; Chichkov, B. N. *Opt. Express* **2009**, *17*, 2143.
(211) Wong, S.; Deubel, M.; Perez-Willard, F.; John, S.; Ozin, G. A.; Wegener, M.; von Freymann, G. *Adv. Mater.* **2006**, *18*, 265.
(212) Kolobov, A. V. Photo-induced Metastability. In *Amorphous Semiconductors*; Wiley-VCH: Weinheim, Germany, 2003.
(213) Sun, H. B.; Nakamura, A.; Kaneko, K.; Shoji, S.; Kawata, S. *Opt. Lett.* **2005**, *30*, 881.
(214) Scrimgeour, J.; Sharp, D. N.; Blanford, C. F.; Roche, O. M.; Denning, R. G.; Turberfield, A. J. *Adv. Mater.* **2006**, *18*, 1557.
(215) Ramanan, V.; Nelson, E.; Brzezinski, A.; Braun, P. V.; Wiltzius, P. *Appl. Phys. Lett.* **2008**, *92*, 173304.
(216) Braun, P. V.; Rinne, S. A.; Garcia-Santamaria, F. *Adv. Mater.* **2006**, *18*, 2665.
(217) Arsenault, A.; Fleischhaker, F.; von Freymann, G.; Kitaev, V.; Miguez, H.; Mihi, A.; Tetreault, N.; Vekris, E.; Manners, I.; Aitchison, S.; Perovic, D.; Ozin, G. A. *Adv. Mater.* **2006**, *18*, 2779.
(218) Rinne, S. A.; Garcia-Santamaria, F.; Braun, P. V. *Nat. Photonics* **2008**, *2*, 52.
(219) Nelson, E. C.; García-Santamaría, F.; Braun, P. V. *Adv. Funct. Mater.* **2008**, *18*, 1983.
(220) Wijnhoven, J.; Bechger, L.; Vos, W. L. *Chem. Mater.* **2001**, *13*, 4486.
(221) Braun, P.; Wiltzius, P. *Adv. Mater.* **2001**, *13*, 482.
(222) Blanco, A.; Chomski, E.; Grabtchak, S.; Ibisate, M.; John, S.; Leonard, S. W.; Lopez, C.; Meseguer, F.; Miguez, H.; Mondia, J. P.; Ozin, G. A.; Toader, O.; van Driel, H. M. *Nature* **2000**, *405*, 437.
(223) Vlasov, Y. A.; Bo, X. Z.; Sturm, J. C.; Norris, D. J. *Nature* **2001**, *414*, 289.
(224) Miguez, H.; Tetreault, N.; Yang, S. M.; Kitaev, V.; Ozin, G. A. *Adv. Mater.* **2003**, *15*, 597.
(225) Tétreault, N.; Miguez, H.; Ozin, G. A. *Adv. Mater.* **2004**, *16*, 1471.
(226) Tétreault, N.; von Freymann, G.; Deubel, M.; Hermatschweiler, M.; Perez-Willard, F.; John, S.; Wegener, M.; Ozin, G. A. *Adv. Mater.* **2006**, *18*, 457.
(227) Miguez, H.; Meseguer, F.; Lopez, C.; Holgado, M.; Andreasen, G.; Mifsud, A.; Fornes, V. *Langmuir* **2000**, *16*, 4405.
(228) Miguez, H.; Chomski, E.; Garcia-Santamaria, F.; Ibisate, M.; John, S.; Lopez, C.; Meseguer, F.; Mondia, J. P.; Ozin, G. A.; Toader, O.; van Driel, H. M. *Adv. Mater.* **2001**, *13*, 1634.
(229) García-Santamaría, F.; Xu, M. J.; Lousse, V.; Fan, S. H.; Braun, P. V.; Lewis, J. A. *Adv. Mater.* **2007**, *19*, 1567.
(230) García-Santamaría, F.; Ibisate, M.; Rodriguez, I.; Meseguer, F.; Lopez, C. *Adv. Mater.* **2003**, *15*, 788.
(231) King, J. S.; Graugnard, E.; Summers, C. J. *Adv. Mater.* **2005**, *17*, 1010.
(232) King, J. S.; Heineman, D.; Graugnard, E.; Summers, C. J. *Appl. Surf. Sci.* **2005**, *244*, 511.
(233) King, J. S.; Graugnard, E.; Roche, O. M.; Sharp, D. N.; Scrimgeour, J.; Denning, R. G.; Turberfield, A. J.; Summers, C. J. *Adv. Mater.* **2006**, *18*, 1561.
(234) King, J. S.; Gaillot, D. P.; Graugnard, E.; Surnmers, C. J. *Adv. Mater.* **2006**, *18*, 1063.
(235) Graugnard, E.; King, J. S.; Gaillot, D. P.; Summers, C. J. *Adv. Funct. Mater.* **2006**, *16*, 1187.
(236) Dong, W. T.; Bongard, H.; Tesche, B.; Marlow, F. *Adv. Mater.* **2002**, *14*, 1457.
(237) Dong, W. T.; Bongard, H. J.; Marlow, F. *Chem. Mater.* **2003**, *15*, 568.
(238) Galusha, J. W.; Tsung, C. K.; Stucky, G. D.; Bartl, M. H. *Chem. Mater.* **2008**, *20*, 4925.
(239) Xu, Y.; Zhu, X.; Dan, Y.; Moon, J. H.; Chen, V. W.; Johnson, A. T.; Perry, J. W.; Yang, S. *Chem. Mater.* **2008**, *20*, 1816.
(240) Hetherington, N. B. J.; Kulak, A. N.; Sheard, K.; Meldrum, F. C. *Langmuir* **2006**, *22*, 1955.
(241) Yue, W. B.; Kulak, A. N.; Meldrum, F. C. *J. Mater. Chem.* **2006**, *16*, 408.
(242) Holland, B. T.; Blanford, C. F.; Do, T.; Stein, A. *Chem. Mater.* **1999**, *11*, 795.
(243) Zhao, X. S.; Su, F. B.; Yan, Q. F.; Guo, W. P.; Bao, X. Y.; Lv, L.; Zhou, Z. C. *J. Mater. Chem.* **2006**, *16*, 637.
(244) Stein, A.; Li, F.; Denny, N. R. *Chem. Mater.* **2008**, *20*, 649.
(245) Guliants, V. V.; Carreon, M. A.; Lin, Y. S. *J. Membr. Sci.* **2004**, *235*, 53.
(246) Li, Y. H.; Zeng, D. M.; Huang, K. L. *Prog. Chem.* **2008**, *20*, 245.
(247) Galisteo, J. F.; Garcia-Santamaria, F.; Golmayo, D.; Juarez, B. H.; Lopez, C.; Palacios, E. *J. Opt. A* **2005**, *7*, S244.
(248) Marlow, F.; Dong, W. T. *ChemPhysChem* **2003**, *4*, 549.
(249) Busch, K.; John, S. *Phys. Rev. E* **1998**, *58*, 3896.
(250) Dong, W.; Marlow, F. *Microporous Mesoporous Mater.* **2007**, *99*, 236.
(251) Moon, J. H.; Xu, Y. G.; Dan, Y. P.; Yang, S. M.; Johnson, A. T.; Yang, S. *Adv. Mater.* **2007**, *19*, 1510.
(252) Miguez, H.; Tetreault, N.; Hatton, B.; Yang, S. M.; Perovic, D.; Ozin, G. A. *Chem. Commun.* **2002**, 2736.
(253) Wang, H.; Yang, Z. Y.; Lu, Y. F. *J. Appl. Phys.* **2007**, *101*, 5.

(254) Wang, H.; Lu, Y. F. *J. Appl. Phys.* **2008**, *103*.
(255) Suntola, T.; Simpson, M. *Atomic Layer Epitaxy*; Chapman and Hall: New York, 1990.
(256) Yue, W. B.; Park, R. J.; Kulak, A. N.; Meldrum, F. C. *J. Cryst. Growth* **2006**, *294*, 69.
(257) Lai, M.; Kulak, A. N.; Law, D.; Zhang, Z. B.; Meldrum, F. C.; Riley, D. J. *Chem. Commun.* **2007**, 3547.
(258) Holland, B. T.; Blanford, C. F.; Stein, A. *Science* **1998**, *281*, 538.
(259) Wang, D. Y.; Caruso, R. A.; Caruso, F. *Chem. Mater.* **2001**, *13*, 364.
(260) McHugh, M. A.; Krukonis, V. J. *Supercritical Fluid Extraction Principles and Practice*; Butterworth: Stoneham, MA, 1994.
(261) Spuhl, O.; Herzog, S.; Gross, J.; Smirnova, I.; Arlt, W. *Ind. Eng. Chem. Res.* **2004**, *43*, 4457.
(262) Cabanas, A.; Enciso, E.; Carbajo, M. C.; Torralvo, M. J.; Pando, C.; Renuncio, J. A. R. *Chem. Mater.* **2005**, *17*, 6137.
(263) Sui, R. H.; Rizkalla, A. S.; Charpentier, P. A. *Cryst. Growth Des.* **2008**, *8*, 3024.
(264) Cabanas, A.; Enciso, E.; Carbajo, M. C.; Torralvo, M. J.; Pando, C.; Renuncio, J. A. R. *Langmuir* **2006**, *22*, 8966.
(265) Braun, P. V.; Wiltzius, P. *Nature* **1999**, *402*, 603.
(266) Miao, Z.; Xu, D. S.; Ouyang, J. H.; Guo, G. L.; Zhao, X. S.; Tang, Y. Q. *Nano Lett.* **2002**, *2*, 717.
(267) Yan, H. W.; Yang, Y. L.; Fu, Z. P.; Yang, B. F.; Xia, L. S.; Fu, S. Q.; Li, F. Q. *Electrochem. Commun.* **2005**, *7*, 1117.
(268) Li, W. J.; Sun, G.; Tang, F. Q.; Tam, W. Y.; Li, J. S.; Chan, C. T.; Sheng, P. *J. Phys.: Condens. Matter* **2005**, *17*, 2177.
(269) Masson, J.-B.; Gallot, G. *Phys. Rev. B* **2006**, *73*, 121401.
(270) Fleming, J. G.; Lin, S. Y.; El-Kady, I.; Biswas, R.; Ho, K. M. *Nature* **2002**, *417*, 52.
(271) Jiang, Y.; Whitehouse, C.; Li, J.; Tam, W. Y.; Chan, C. T.; Sheng, P. *J. Phys.: Condens. Matter* **2003**, *15*, 5871.
(272) Yu, X. D.; Lee, Y. J.; Furstenberg, R.; White, J. O.; Braun, P. V. *Adv. Mater.* **2007**, *19*, 1689.
(273) Andricacos, P. C.; Uzoh, C.; Dukovic, J. O.; Horkans, J.; Deligianni, H. *IBM J. Res. Dev.* **1998**, *42*, 567.
(274) Bao, Z. H.; Weatherspoon, M. R.; Shian, S.; Cai, Y.; Graham, P. D.; Allan, S. M.; Ahmad, G.; Dickerson, M. B.; Church, B. C.; Kang, Z. T.; Abernathy, H. W.; Summers, C. J.; Liu, M. L.; Sandhage, K. H. *Nature* **2007**, *446*, 172.
(275) Richman, E. K.; Kang, C. B.; Brezesinski, T.; Tolbert, S. H. *Nano Lett.* **2008**, *8*, 3075.
(276) Gratson, G. M.; Xu, M. J.; Lewis, J. A. *Nature* **2004**, *428*, 386.
(277) Ekinci, Y.; Solak, H. H.; Padeste, C.; Gobrecht, J.; Stoykovich, M. P.; Nealey, P. F. *Microelectron. Eng.* **2007**, *84*, 700.

CR900080V